REFERENCES

1. Lee P, Wang CC, Adamis AP. Ocular neovascularization: an epidemiologic review. *Surv Ophthalmol.* 1998;43(3):245-269.
2. Leibowitz HM, Krueger DE, Maunder LR, et al. The Framingham Eye Study monograph: an ophthalmological and epidemiological study of cataract, glaucoma, diabetic retinopathy, macular degeneration, and visual acuity in a general population of 2631 adults, 1973-1975. *Surv Ophthalmol.* 1980;24(suppl):335-610.
3. Ishibashi T, Hata Y, Yoshikawa H, Nakagawa K, Sueishi K, Inomata H. Expression of vascular endothelial growth factor in experimental choroidal neovascularization. *Graefes Arch Clin Exp Ophthalmol.* 1997;235(3):159-167.
4. Lopez PF, Sippy BD, Lambert HM, Thach AB, Hinton DR. Transdifferentiated retinal pigment epithelial cells are immunoreactive for vascular endothelial growth factor in surgically excised age-related macular degeneration-related choroidal neovascular membranes. *Invest Ophthalmol Vis Sci.* 1996;37(5):855-868.
5. Yi X, Ogata N, Komada M, et al. Vascular endothelial growth factor expression in choroidal neovascularization in rats. *Graefes Arch Clin Exp Ophthalmol.* 1997; 235(5):313-319.
6. Amin R, Puklin JE, Frank RN. Growth factor localization in choroidal neovascular membranes of age-related macular degeneration. *Invest Ophthalmol Vis Sci.* 1994;35(8):3178-3188.
7. Carmeliet P, Ferreira V, Breier G, et al. Abnormal blood vessel development and lethality in embryos lacking a single VEGF allele. *Nature.* 1996;380(6573):435-439.
8. Folkman J. Angiogenesis in cancer, vascular, rheumatoid and other disease. *Nat Med.* 1995;1(1):27-31.
9. Kvanta A. Expression and regulation of vascular endothelial growth factor in choroidal fibroblasts. *Curr Eye Res.* 1995;14(11):1015-1020.
10. Wada M, Ogata N, Otsuji T, Uyama M. Expression of vascular endothelial growth factor and its receptor (KDR/flk-1) mRNA in experimental choroidal neovascularization. *Curr Eye Res.* 1999;18(3):203-213.
11. de Vries C, Escobedo JA, Ueno H, Houck K, Ferrara N, Williams LT. The fms-like tyrosine kinase, a receptor for vascular endothelial growth factor. *Science.* 1992; 255(5047):989-991.
12. Millauer B, Wizigmann-Voos S, Schnürch H, et al. High affinity VEGF binding and developmental expression suggest Flk-1 as a major regulator of vasculogenesis and angiogenesis. *Cell.* 1993;72(6):835-846.
13. Waltenberger J, Claesson-Welsh L, Siegbahn A, Shibuya M, Heldin CH. Different signal transduction properties of KDR and Flt1, two receptors for vascular endothelial growth factor. *J Biol Chem.* 1994;269(43):26988-26995.
14. Wu LW, Mayo LD, Dunbar JD, et al. Utilization of distinct signaling pathways by receptors for vascular endothelial cell growth factor and other mitogens in the induction of endothelial cell proliferation. *J Biol Chem.* 2000;275(7):5096-5103.
15. Spannuth WA, Sood AK, Coleman RL. Angiogenesis as a strategic target for ovarian cancer therapy. *Nat Clin Pract Oncol.* 2006;5(4):194-204.
16. Fong TA, Shawver LK, Sun L, et al. SU5416 is a potent and selective inhibitor of the vascular endothelial growth factor receptor (Flk-1/KDR) that inhibits tyrosine kinase catalysis, tumor vascularization, and growth of multiple tumor types. *Cancer Res.* 1999;59(1):99-106.
17. Mendel DB, Schreck RE, West DC, et al. The angiogenesis inhibitor SU5416 has long-lasting effects on vascular endothelial growth factor receptor phosphorylation and function. *Clin Cancer Res.* 2000;6(12):4848-4858.
18. Ye C, Sweeny D, Sukbuntherng J, et al. Distribution, metabolism, and excretion of the anti-angiogenic compound SU5416. *Toxicol In Vitro.* 2006;20(2):154-162.
19. Katanasaka Y, Ida T, Asai T, et al. Antiangiogenic cancer therapy using tumor vasculature-targeted liposomes encapsulating 3-(3,5-dimethyl-1H-pyrrol-2-ylmethylene)-1,3-dihydro-indol-2-one, SU5416. *Cancer Lett.* 2008;270(2): 260-268.
20. Maeda N, Miyazawa S, Shimizu K, et al. Enhancement of anticancer activity in antineovascular therapy is based on the intratumoral distribution of the active targeting carrier for anticancer drugs. *Biol Pharm Bull.* 2006;29(9):1936-1940.
21. Maeda N, Takeuchi Y, Takada M, Sadzuka Y, Namba Y, Oku N. Anti-neovascular therapy by use of tumor neovasculature-targeted long-circulating liposome. *J Control Release.* 2004;100(1):41-52.
22. Oku N, Asai T, Watanabe K, et al. Anti-neovascular therapy using novel peptides homing to angiogenic vessels. *Oncogene.* 2002;21(17):2662-2669.
23. Allen TM, Cullis PR. Drug delivery systems: entering the mainstream. *Science.* 2004;303(5665):1818-1822.
24. Ebrahim S, Peyman GA, Lee PJ. Applications of liposomes in ophthalmology. *Surv Ophthalmol.* 2005;50(2):167-182.
25. Demers G, Griffin G, De Vroey G, Haywood JR, Zurlo J, Bédard M. Animal research: harmonization of animal care and use guidance. *Science.* 2006;312 (5774):700-701.
26. Takehana Y, Kurokawa T, Kitamura T, et al. Suppression of laser-induced choroidal neovascularization by oral tranilast in the rat. *Invest Ophthalmol Vis Sci.* 1999;40(2):459-466.
27. Edelman JL, Castro MR. Quantitative image analysis of laser-induced choroidal neovascularization in rat. *Exp Eye Res.* 2000;71(5):523-533.
28. Kami J, Muranaka K, Yanagi Y, Obata R, Tamaki Y, Shibuya M. Inhibition of choroidal neovascularization by blocking vascular endothelial growth factor receptor tyrosine kinase. *Jpn J Ophthalmol.* 2008;52(2):91-98.
29. D'Amato R, Wesolowski E, Smith LE. Microscopic visualization of the retina by angiography with high-molecular-weight fluorescein-labeled dextrans in the mouse. *Microvasc Res.* 1993;46(2):135-142.
30. Zacks DN, Ezra E, Terada Y, et al. Verteporfin photodynamic therapy in the rat model of choroidal neovascularization: angiographic and histologic characterization. *Invest Ophthalmol Vis Sci.* 2002;43(7):2384-2391.
31. Ciulla TA, Criswell MH, Danis RP, Hill TE. Intravitreal triamcinolone acetonide inhibits choroidal neovascularization in a laser-treated rat model. *Arch Ophthalmol.* 2001;119(3):399-404.
32. Fiscella R, Peyman GA, Fishman PH. Duration of therapeutic levels of intravitreally injected liposome-encapsulated clindamycin in the rabbit. *Can J Ophthalmol.* 1987;22(6):307-309.
33. Rao VS, Peyman GA, Khoobehi B, Vangipuram S. Evaluation of liposome-encapsulated clindamycin in *Staphylococcus aureus* endophthalmitis. *Int Ophthalmol.* 1989;13(3):181-185.
34. Fishman PH, Peyman GA, Lesar T. Intravitreal liposome-encapsulated gentamicin in a rabbit model: prolonged therapeutic levels. *Invest Ophthalmol Vis Sci.* 1986;27(7):1103-1106.
35. Zeng S, Hu C, Wei H, et al. Intravitreal pharmacokinetics of liposome-encapsulated amikacin in a rabbit model. *Ophthalmology.* 1993;100(11):1640-1644.
36. Tremblay C, Barza M, Szoka F, Lahav M, Baum J. Reduced toxicity of liposome-associated amphotericin B injected intravitreally in rabbits. *Invest Ophthalmol Vis Sci.* 1985;26(5):711-718.
37. Liu KR, Peyman GA, Khoobehi B. Efficacy of liposome-bound amphotericin B for the treatment of experimental fungal endophthalmitis in rabbits. *Invest Ophthalmol Vis Sci.* 1989;30(7):1527-1534.
38. Alghadyan AA, Peyman GA, Khoobehi B, Milner S, Liu KR. Liposome-bound cyclosporine: clearance after intravitreal injection. *Int Ophthalmol.* 1988;12(2): 109-112.
39. Joondeph BC, Peyman GA, Khoobehi B, Yue BY. Liposome-encapsulated 5-fluorouracil in the treatment of proliferative vitreoretinopathy. *Ophthalmic Surg.* 1988; 19(4):252-256.
40. Fishman P, Peyman GA, Hendricks R, Hui SL. Liposome-encapsulated 3H-5FU in rabbits. *Int Ophthalmol.* 1989;13(5):361-365.
41. Takeda A, Hata Y, Shiose S, et al. Suppression of experimental choroidal neovascularization utilizing KDR selective receptor tyrosine kinase inhibitor. *Graefes Arch Clin Exp Ophthalmol.* 2003;241(9):765-772.
42. Shimotake J, Derugin N, Wendland M, Vexler ZS, Ferriero DM. Vascular endothelial growth factor receptor-2 inhibition promotes cell death and limits endothelial cell proliferation in a neonatal rodent model of stroke. *Stroke.* 2010; 41(2):343-349.

International Journal of Pharmaceutics 403 (2011) 170–177

Contents lists available at ScienceDirect

International Journal of Pharmaceutics

journal homepage: www.elsevier.com/locate/ijpharm

Pharmaceutical Nanotechnology

PET imaging of brain cancer with positron emitter-labeled liposomes

Naoto Oku[a,*], Mina Yamashita[a], Yurie Katayama[a], Takeo Urakami[a,1], Kentaro Hatanaka[a], Kosuke Shimizu[a], Tomohiro Asai[a], Hideo Tsukada[b], Shuji Akai[c], Hiroaki Kanazawa[d]

[a] Department of Medical Biochemistry and Global COE, Graduate School of Pharmaceutical Sciences, University of Shizuoka, Yada, Suruga-ku, Shizuoka 422-8526, Japan
[b] PETCenter, Central Research Laboratory, Hamamatsu Photonics K.K. Hirakuchi, Hamakita-ku, Hamamatu, Shizuoka 434-8601, Japan
[c] Department of Synthetic Organic Chemistry, Graduate School of Pharmaceutical Sciences, University of Shizuoka, Yada, Suruga-ku, Shizuoka 422-8526, Japan
[d] Department of Anatomy, School of Nursing, University of Shizuoka, Yada, Suruga-ku, Shizuoka 422-8526, Japan

ARTICLE INFO

Article history:
Received 6 May 2010
Received in revised form
30 September 2010
Accepted 2 October 2010
Available online 8 October 2010

Keywords:
Positron emission tomography
Brain cancer
Liposome
Cancer diagnosis
Passive targeting
Angiogenesis

ABSTRACT

Since nanocarriers such as liposomes are known to accumulate in tumors of tumor-bearing animals, and those that have entrapped a positron emitter can be used to image a tumor by PET, we applied ^{18}F-labeled 100-nm-sized liposomes for the imaging of brain tumors. Polyethylene glycol (PEG)-modified liposomes, which are known to accumulate in tumors by passive targeting and those modified with Ala-Pro-Arg-Pro-Gly, which are known to home into angiogenic sites were used. Those liposomes labeled with DiI fluorescence accumulated in a glioma implanted in a rat brain 1 h after the injection, although they did not accumulate in the normal brain tissues due to the protection afforded by the blood–brain barrier. Preformed liposomes were easily labeled with 1-[^{18}F]fluoro-3,6-dioxatetracosane, and enabled the imaging of gliomas by PET with higher contrast than that obtained with [^{18}F]deoxyfluoroglucose. In addition, the smallest tumor among those tested, having a diameter of 1 mm was successfully imaged by the liposomal ^{18}F. Therefore, nanocarrier-based imaging of brain tumors is promising for the diagnosis of brain cancer and possible drug delivery-based therapy.

1. Introduction

Brain cancers such as glioblastomas are known to be aggressive and invasive (Wen and Kesari, 2008). Therefore, diagnosis of brain cancer at the early stages is quite important. Positron emission tomography (PET) is one of the strong tools for diagnosis, therapeutic evaluation, and prognostic evaluation of cancer. [2-^{18}F]-2-deoxyfluoro-D-glucose (FDG) is the most widely used positron emitter for cancer diagnosis (Scott et al., 2008; Nakamoto et al., 2009). However, the utility of FDG-PET imaging for detection of brain cancer is controversial due to the high demand for glucose in the brain (Takeda et al., 2003; Chen, 2007). To reduce this bothersome background various compounds such as [^{11}C]choline (Tian et al., 2004; Kato et al., 2008), [^{11}C]acetate (Yamamoto et al., 2008), and amino acid analogues such as [^{11}C]methionine (Hatakeyama et al., 2008; Jager et al., 2001), L-[methyl-^{11}C]methionine (Nojiri et al., 2009; Ullrich et al., 2009), *O*-[^{11}C]methyl-L-tyrosine (Ishiwata et al., 2004), *O*-[^{18}F]fluoromethyl-L-tyrosine (Ishiwata et al., 2004), *O*-[^{18}F]fluoroethyl-L-tyrosine (Heiss et al., 1999; Langen et al., 2006; Floeth et al., 2007; Mehrkens et al., 2008; Pauleit et al., 2009), and *O*-[^{18}F]fluoropropyl-L-tyrosine (Tang et al., 2003) have been synthesized and evaluated as PET imaging agents for the diagnosis and detection of recurrence of brain tumors. Among them, the amino acid analogues show relatively low accumulation in normal peripheral tissue (low tissue-to-blood ratio) and rapid blood clearance and have been used for detecting brain tumors and other tumors as well. We also demonstrated that the D-amino acid analogue *O*-[^{18}F]fluoromethyl-D-tyrosine is useful for tumor imaging by PET (Urakami et al., 2009).

Nanomedicines such as liposomal drugs are known to accumulate in tumors due to the enhanced permeability of tumor blood vessels and the retention effect (Maeda et al., 2000, 2009). This drug delivery system (DDS) strategy is based on the nature of tumors: tumor cells demand oxygen and nutrition and cause angiogenesis for obtaining them, and angiogenic vessels are leaky enough to be permeated by nano-sized materials. Liposomes are known as one of the most effective drug carriers for cancer therapy. In liposomal DDS technologies, polyethylene glycol (PEG)-modified liposomes are useful drug carriers for cancer therapy; for they have a characteristically long circulation time in the bloodstream due to avoidance of being trapped by the reticuloendothelial system (RES) such as in the liver and spleen (Sakakibara et al., 1996;

* Corresponding author. Tel.: +81 54 264 5701; fax: +81 54 264 5705.
E-mail address: oku@u-shizuoka-ken.ac.jp (N. Oku).
[1] Present address: The Burnham Institute for Medical Research at Lake Nona, 6400 Sanger Rd., Orlando, FL 32827, United States.

0378-5173/$ – see front matter © 2010 Elsevier B.V. All rights reserved.
doi:10.1016/j.ijpharm.2010.10.001

Gabizon, 2001). PEG-modified liposomes tend to accumulate in tumor tissues through passive targeting, and PEG-modified liposomes containing doxorubicin have been used in clinical cancer therapy.

We previously demonstrated that PEG-liposomes encapsulating [^{18}F]FDG accumulate in solid tumors and can be effectively imaged by PET (Oku et al., 1996). Although the encapsulation efficiency of [^{18}F]FDG is not so high, the result indicated the usefulness of liposomes or nanocarriers for cancer imaging. Moreover, actively targeting nanocarriers specifically associating with tumor cells or angiogenic vessels are an attractive approach. For example, we previously demonstrated that liposomes modified with a peptide specifically recognized by membrane type-1 matrix metalloproteinase (MT1-MMP), which is expressed on the surface of angiogenic endothelial cells, accumulate in tumors (Kondo et al., 2004). In that study, we encapsulated [^{18}F]FDG in the liposomes and determined the distribution of the liposomes by PET. We also performed *in vivo* biopanning of a phage-displayed peptide library using an angiogenesis mouse model to obtain specific probes for angiogenic endothelial cells, and identified the Ala-Pro-Arg-Pro-Gly (APRPG) motif as a novel peptide homing to angiogenic vessels (Oku et al., 2002; Asai et al., 2002). Liposomes modified with APRPG and labeled with [^{3}H]cholesterol hexadecylether actually accumulate in tumors of colon 26 NL-17 carcinoma-implanted mice (Maeda et al., 2004). Moreover, the accumulation of APRPG-modified liposomes in such tumors was also confirmed by PET analysis using [^{18}F]FDG-encapsulated liposomes (Maeda et al., 2006).

In the present study, we applied PEG-modified and APRPG–PEG-modified liposomes entrapping a positron-emitter to brain tumor imaging by PET. At first, we analyzed distribution of fluorescence-labeled liposomes in glioma-bearing brain of rats by use of fluorescence microscopy and an *in vivo* fluorescence-based imaging system. Then PET imaging of brain cancers was achieved by use of 1-[^{18}F]fluoro-3,6-dioxatetracosane ([^{18}F]SteP2)-labeled liposomes. Our results indicate that even a 1-mm diameter brain tumor could be imaged by PET, thus demonstrating the usefulness of these liposomes for PET imaging of brain cancer.

2. Materials and methods

2.1. Preparation of liposomes

All lipids were the products of Nippon Fine Chemical, Co. Ltd. (Takasago, Hyogo, Japan). Distearoylphosphatidylcholine (DSPC) and cholesterol along with DSPE–PEG or DSPE–PEG–APRPG (10:5:1 as a molar ratio) were dissolved in chloroform/*t*-butanol to formulate PEG-modified liposomes (PEG-liposomes) or APRPG–PEG-modified liposomes (APRPG-liposomes), respectively. For fluorescence labeling of liposomes, 1,1′-dioctadecyl-3,3,3′,3′-tetramethyl-indocarbocyanine perchlorate (DiI, Molecular Probes Inc., Eugene, OR, USA) was added to the initial chloroform/*t*-butanol solution at a concentration of 1 mol% of DSPC. After the lipids had been dried under reduced pressure and stored *in vacuo* for at least 1 h, liposomes were prepared by hydration of the thin lipid film with 0.3 M glucose solution and frozen and thawed for 3 cycles by using liquid nitrogen. Then, the liposomes were sized by extruding them thrice through a polycarbonate membrane filter with 100-nm pores (Nuclepore track-Etch Membrane, Lipex). Particle size and ζ-potential of PEG-liposomes and APRPG-liposomes were measured by use of a Zetasizer Nano ZS (MALVERN, Worcestershire UK, USA) and found to be 113 nm and −2.0 mV, respectively, for PEG-liposomes and 107 nm and −3.3 mV, respectively, for the APRPG-liposomes.

2.2. Preparation of brain cancer-bearing model rats

The glioma-bearing rat model was prepared by a modification of the procedure described previously (Takeda et al., 2003). Nine-week-old Fischer 344 male rats (Japan SLC, Hamamatsu, Japan) were cared for according to the Animal Facility Guidelines of the University of Shizuoka. For the implantation of tumor cells, the rats were anesthetized with chloral hydrate (40 mg/kg) in saline and individually placed in a stereotaxic apparatus. C6 glioma cells were maintained in Dulbecco's modified Eagle medium (DMEM, Wako Fine Chemical Co. Ltd., Osaka, Japan) supplemented with 10% heat-inactivated fetal bovine serum (Japan Bioserum Co. Ltd., Japan), penicillin G (100 U/mL) and streptomycin (100 μg/mL) at 37 °C in 5% CO_2 atmosphere. After harvesting of these cells, the cells were suspended in DMEM containing 1% gelatin (2×10^7 cells/mL). Ten microliters of the cell suspension or vehicle (DMEM containing 1% gelatin) was injected at a rate of 0.7 μL/min into the left midbrain of each rat (4.3 mm posterior to bregma, 3.9 mm lateral to the midline suture, and 7.0 mm in depth) with an infusion pump (11 Plus, Harvard Apparatus, USA).

2.3. Intratumoral localization of DiI-labeled liposomes

C6 glioma cells (2.0×10^5 cells/rat) were inoculated as described above. DiI-labeled liposomes were administered via a tail vein of the rat at 11 days after tumor implantation. One hour or 24 h after the injection of liposomes (0.5 mL/rat, 5 μmol as DSPC), the rats were anesthetized with chloral hydrate, perfused with *ca.* 200 mL saline and with *ca.* 100 mL 20% formaldehyde for the fixation. The brain was removed and sliced at a 2-mm thickness with a cryostat microtome (HM 505E, Microm, Walldorf, Germany). The slices were then incubated twice in PBS for 4 h each time at 4 °C, and then overnight in 30% sucrose solution at 4 °C. After removal of water, the slices were embedded in optimal cutting temperature compound (Sakura Finetech, Co. Ltd., Tokyo, Japan) and frozen at −80 °C. Brain sections (10 μm) were prepared with a cryostat microtome, and mounted on MAS-coated slides (Matsunami Glass Ind., Ltd., Japan) for observation with a fluorescence microscope (IMT-2, Olympus, Japan). Then, the slices were stained with hematoxylin and eosin (HE) and observed under the microscope.

2.4. Ex vivo imaging of the distribution of DiI-labeled liposomes

DiI-labeled liposomes (0.5 mL/rat, 5 μmol as DSPC) were administered via a tail vein of a rat at 9 days after the implantation of C6 glioma cells. One hour after the injection, the rats were sacrificed; and brain slices (2-mm thickness) were then prepared with a cryostat microtome without perfusion and fixation. Fluorescent images of those slices were obtained with a fluorescence imaging system (IVIS Lumina, Xenogen).

2.5. Preparation of positron emitter-labeled liposomes

Preparation of 1-[^{18}F]fluoro-3,6-dioxatetracosane (SteP2) and liposome labeling by the SophT method were performed as described previously (Urakami et al., 2007). About 100 MBq of [^{18}F]SteP2 in ethanol solution was transferred to a glass test tube, and the solvent was removed completely at 90 °C with a helium gas flow. Liposomal solution (1 mL, 10 μmol as DSPC) was added to the vial having a thin film of ^{18}F-radiolabeled compound and incubated at 65 °C for 15 min with 5-s mixing by a vortex stirrer every 3 min. After the incubation, the liposomal solution was washed with PBS by centrifugation at 100,000 × *g* for 15 min (Beckman, Fullerton, CA, USA), and the pellet was resuspended and diluted in PBS to make a 22 MBq/mL solution. Radioactivity was measured with a curie meter (IGC-3, Aloka, Japan).

Rats anesthetized with chloral hydrate at 11 days after the implantation of C6 glioma cells were placed on an animal CT (Clairvivo CT, Shimadzu, Japan) to obtain CT images. Then, [^{18}F]SteP2-labeled liposomes (10 MBq/rat) were administered via a tail vein. PET scans were started immediately after the injection and continued for 60 min by use of an animal PET apparatus (Clairvivo PET, Shimadzu, Japan).

FDG-PET was similarly performed. [^{18}F]FDG (10 MBq/rat) was injected into the rats after having obtained the CT images.

2.6. PET analysis and autoradiography

Before PET analysis, rats anesthetized with chloral hydrate at 11 days after the implantation of C6 glioma cells were placed on the animal CT to obtain CT images. Then, [^{18}F]SteP2-labeled liposomes (10 MBq/rat) were administered via a tail vein. Then the PET scan was started immediately after the injection and continued for 60 min. FDG-PET was similarly performed. [^{18}F]FDG (10 MBq/rat) was injected into the rats after having obtained the CT images.

After the PET scan, the rats were sacrificed; and the brain was then excised. Thereafter, 2-mm slices were prepared and set on an imaging plate. Autoradiograms were obtained by using a bioimaging analyzer system (BAS2000, Fuji Film, Japan).

2.7. Biodistribution of liposomes

Glioma-bearing rats were injected with [^{18}F]SteP2-labeled PEG-liposomes (10 MBq/rat) via a tail vein as described above. At 1 h after the injection, the rats were sacrificed, and blood and organs (heart, lung, liver, spleen kidney normal part of brain, brain tumor) were removed. The radioactivity of blood and each organ was measured by using an auto gamma counter (1480 Wizard 3, Perkin Elmer, USA).

2.8. Statistical analysis

Differences between groups were evaluated by analysis of variance (ANOVA) with the Tukey *post hoc* test.

3. Results

3.1. Intratumoral distribution of fluorescence-labeled PEG- and APRPG-liposomes

At first, we confirmed that the angiogenic vessels formed by experimental glioma in the rat brain were leaky enough to allow permeation by nanomedicines such as liposomes. As shown in Fig. 1B and E, the DiI fluorescence of DiI-labeled PEG-liposomes and APRPG-liposomes, respectively, was observed in the glioma at 1 h after intravenous injection of the liposomes. Since DiI fluorescence was not observed in the normal brain tissues near the tumor, we concluded that the liposomes had accumulated in the tumor through angiogenic vessels. The fluorescence intensity was increased at 24 h after the injection (Fig. 1C and F). Interestingly, the DiI fluorescence of the PEG-liposomes accumulated widely in the tumor, although that of APRPG-liposomes accumulated intensely in rather specific areas, suggesting that these liposomes had accumulated in the angiogenic vessels. These patterns of liposomal fluorescence are consistent with our previous data obtained by use of tumor-bearing mice that had been implanted subcutaneously with C26 NL-17 colon carcinoma (Maeda et al., 2006).

To understand the structure of the brain vasculature, we examined normal and glioma-implanted brain specimens after HE-staining. As shown in Fig. 2, capillaries in the normal brain tissue were covered with astrocytes (Fig. 2A); whereas capillaries in the brain tumor tissues were surrounded directly by glioma cells (Fig. 2B). These results support the idea that the blood–brain barrier (BBB) is immature in angiogenic vessels of brain tumors. The possible architecture based on our observation and the literature (Standring, 2005) is shown in Fig. 2C and D.

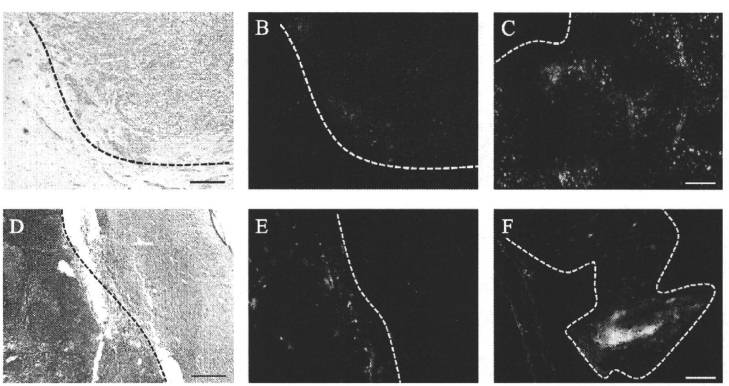

Fig. 1. Intratumoral distribution of fluorescence-labeled liposomes in brain tumor after intravenous injection. Rats were intravenously injected with DiI-labeled PEG-liposomes (A–C) or APRPG-liposomes (D–F) at day 11 after implantation of C6 glioma cells into the left midbrain. At 1 h (A, B, D, and E) or 24 h (C and F) after the injection, the brain tumors were dissected; and 10-μm frozen sections were prepared as described in Section 2. Then, liposomal distribution in the brain was observed under a fluorescence microscope (B, C, E, and F). Red fluorescence shows the liposomal localization. A and D show the images stained with hematoxylin and eosin, corresponding to the fluorescent images of "B" and "E", respectively. The dotted lines show the borders between normal and tumor tissue. Deep purple regions in "A" and "D" indicate the tumor tissues. The scale bar represents 100 μm.

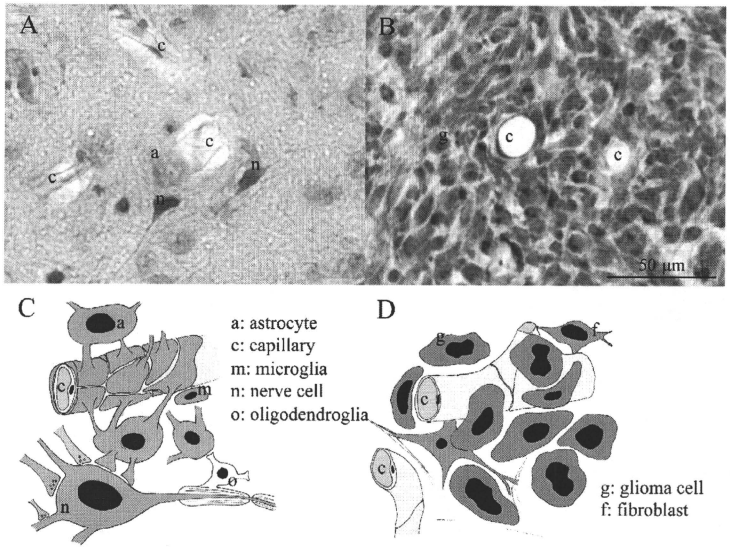

Fig. 2. Structure around blood capillaries in normal brain and brain tumor tissues. A rat brain tumor model was prepared by the implantation of C6 glioma cells into the left midbrain. The brain was dissected, and 10-μm sections of normal right brain (A) and tumor-implanted left brain (B) were stained with hematoxylin and eosin. Schematic interpretation of the histology around blood capillaries in normal brain (C) and brain tumor tissues (D) are shown.

3.2. Ex vivo study on the accumulation of fluorescence-labeled liposomes in brain tumor

Although microscopic study provided data on the intratumoral distribution of the liposomes, the liposomal distribution in the whole brain could not be understood. Therefore, we next examined the distribution of DiI-labeled liposomes in the glioma-bearing brain by use of whole-brain slices. As a result, both PEG-liposomes and APRPG-liposomes accumulated in the brain tumor 1 h after the injection via a tail vein (Fig. 3B and D, respectively). No specific accumulation could be observed in the sham-operated brain after the injection of the DiI-labeled PEG-liposomes (Fig. 3E and F). The fluorescence intensity of the tumor region was 4.0-fold and 3.1-fold higher than that of the contralateral regions after the injection of DiI-labeled PEG-liposomes and DiI-labeled APRPG-liposomes, respectively.

3.3. Brain tumor imaging with positron-emitter-labeled liposomes by PET

Finally, PEG-liposomes and APRPG-liposomes were labeled with the positron emitter [^{18}F]SteP2, by the SophT method, and injected into the glioma-bearing mice. As shown in Fig. 4, the positron emitter accumulated in the tumor region and imaged the tumor after injection in PEG-liposomes (Fig. 4, top panel) or APRPG-liposomes (Fig. 4, middle panel). Interestingly, the other regions of the brain showed a low background. On the contrary, [^{18}F]FDG imaged the whole brain, although the accumulation was higher in the tumor region (Fig. 4, bottom panel). BAS images (autoradiograms) shown in right panel confirmed the region of tumor. The tumor sizes of preparations varied to some extent in the present experiment, and the smallest tumor was revealed to be only about 1 mm in diameter. Interestingly, this small tumor was imaged by PET but was hardly detectable by CT when [^{18}F]SteP2-labeled APRPG-liposomes had been injected (Fig. 5).

The biodistribution of ^{18}F at 1 h after the injection of [^{18}F]SteP2-labeled PEG-liposomes or [^{18}F]FDG is shown in Fig. 6. The liposome-bearing label was maintained in the bloodstream and highly accumulated in the spleen. This result is consistent with our previous study (Maeda et al., 2004). In the brain, ^{18}F in the liposomes or as FDG significantly accumulated more in the tumor than in the normal tissues. In contrast to the distribution of ^{18}F after injection of liposomes bearing it, ^{18}F as FDG was cleared from the bloodstream quite fast and accumulated in the heart and normal region of brain.

4. Discussion

Since the usefulness of FDG-PET for the detection of brain tumors is controversial (Takeda et al., 2003; Chen, 2007), other PET imaging agents have been developed. In the present study, we aimed at imaging brain tumors not by the synthesis of molecules specifically taken up by tumor cells, but by use of DDS technology. Nanocarriers such as liposomes are well known to accumulate in solid tumors, especially in hypervascular tumors, due to the EPR effect (Maeda et al., 2000, 2009). In fact, liposomal radionuclides show effective tumor imaging (Oku et al., 1996; Geng et al., 2004; Elbayoumi and Torchilin, 2006). Moreover, liposome-based radionuclide delivery is not only useful for cancer imaging but also for cancer therapy when the carriers entrapping radiopharmaceuticals or other anticancer agents are used (Kostarelos and

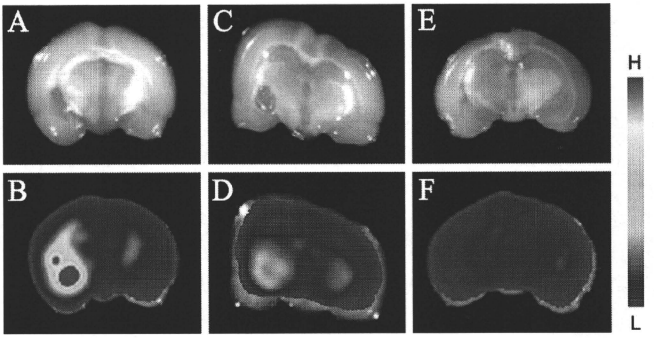

Fig. 3. *Ex vivo* imaging of liposomal distribution in rat brain bearing glioma. Rats were intravenously injected with DiI-labeled PEG-liposomes (A, B, E, and F) or APRPG-liposomes (C and D) at day 9 after implantation of C6 glioma cells (A–D) or medium alone (E and F) into the left midbrain. At 1 h after the injection, the brains were sliced into 2-mm sections, and the distribution of liposomes labeled with DiI was scanned with a fluorescence imaging system, IVIS (B, D, and F). Photos are also shown (A, C, and E). Two separate experiments gave similar results.

Emfietzoglou, 2000; Syme et al., 2003; Hamoudeh et al., 2008). Another advantage of carrier-based imaging is the active targeting by modifying carriers with some specific probes. We previously modified liposomes with angiogenic vessel-specific peptides and observed the efficient delivery of targeting liposomes to cancer by PET (Kondo et al., 2004; Maeda et al., 2006). Therefore, cancer imaging with DDS technology has various advantages including cancer treatment.

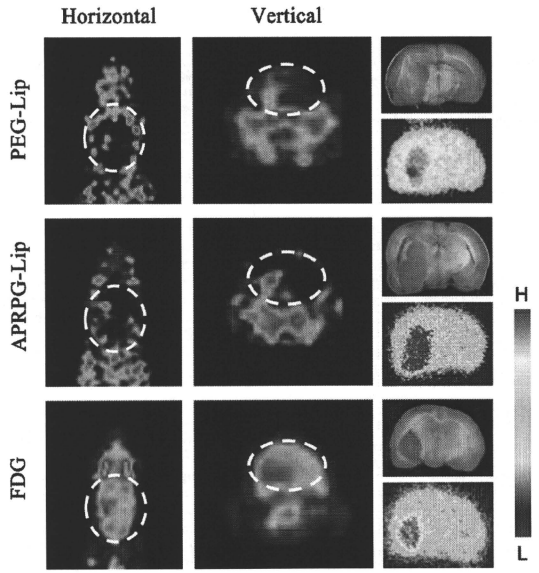

Fig. 4. PET imaging of brain tumor with [^{18}F]SteP2-liposomes and [^{18}F]-FDG. Rats were intravenously injected with 10 MBq of [^{18}F]SteP2-labeled PEG-liposomes (top panel), [^{18}F]SteP2-labeled APRPG-liposomes (middle panel) or [^{18}F]FDG (bottom panel) at day 11 after implantation of C6 glioma cells into the left midbrain. The biodistribution pattern of samples was determined by taking 1 frame/min for 1 h with the Clairvivo PET, and averaged data from 40 to 60 min are shown. Horizontal (left panel) and vertical (center panel) images are shown. After PET imaging, the brains were sliced into 2-mm sections, and the autoradiograms (right lower panels) were obtained with a bioimaging analyzer BAS 2000, and the pictures were taken (right upper panels). The ovals formed by the white dotted line show the estimated brain position.

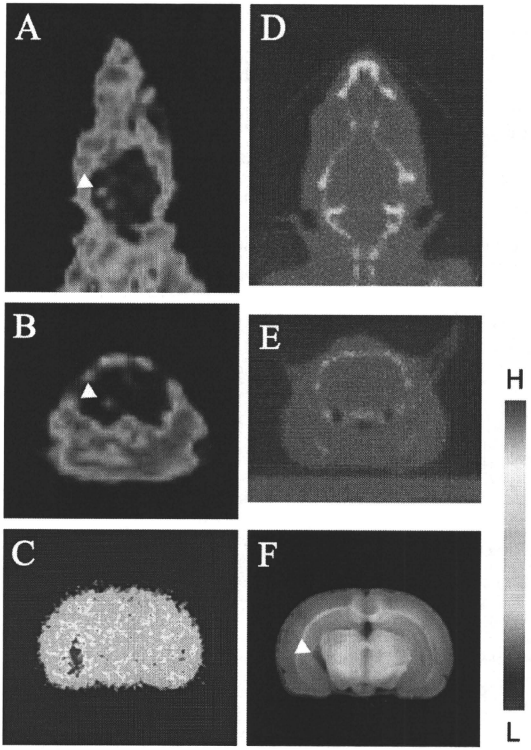

Fig. 5. PET imaging of small brain tumor with [^{18}F]SteP2-liposomes. PET imaging was performed as described in the legend of Fig. 4. Even the smallest tumor, 1-mm diameter, seen among the prepared model rats was imaged by PET. PET images (A and B) and CT images (D and E) of a rat brain are shown. Horizontal (A and D) and vertical (B and E) images are shown. (C) BAS image of a rat brain slice. (F) Photo of the brain slice. Arrowheads indicate the tumor.

It is well known that glioblastoma, the most prevalent brain cancer, is a hypervascular tumor due to angiogenesis (Verhoeff et al., 2009; Brastianos and Batchelor, 2009); and thus nanocarriers such as liposomes would be expected to accumulate in the brain cancer, since the permeability of tumor angiogenic vessels was higher than that of normal blood vessels. Moreover, brain blood vessels especially protect from the penetration of some molecules due to the BBB. Therefore, liposomes or other nanocarriers would be specifically accumulated into brain tumor region after circulating bloodstream, and be useful for brain cancer imaging. For labeling nanocarriers quite conveniently with PET probes, we previously synthesized a novel ^{18}F-labeled amphiphilic compound known as 1-[^{18}F]fluoro-3,6-dioxatetracosane (Urakami et al., 2007). There are several methods for labeling liposomes, although radionuclides need to be incorporated during formulation of the liposomes in most of those methods. For example, to label liposomes with [^{18}F]FDG, [^{18}F]FDG was incorporated into liposomal aqueous phase during hydration step of liposomal lipids. In addition, the encapsulation efficiency of [^{18}F]FDG into the liposomes was very low. The advantage of the "solid-phase transition" (SophT) method is that it is applicable to preformed liposomes with quite high labeling efficiency. Moreover, [^{18}F]SteP2 in DSPC-based liposomes is stable in the presence of serum (Urakami et al., 2007). This universal method of liposomal modification can be used for various kinds of liposomes and lipidic nanoparticles and bring the enhanced detection of a target tissue.

Aim of the present study is to demonstrate the application of positron-labeled liposomes for brain tumor imaging by PET. We firstly examined the intratumoral distribution of fluorescence-labeled PEG- and APRPG-liposomes by fluorescence microscopy, and observed the accumulation of both DiI-labeled PEG-liposomes and APRPG-liposomes in the brain tumor region at 1 h after intravenous injection of the liposomes, although the intratumoral distribution of each liposome was different. We previously demonstrated that PEG-liposomes were accumulated around neovessels and fluorescence of DiI-labeled-APRPG-liposomes was colocalized with CD31 stain in colon 26 NL-17 solid tumor (Maeda et al., 2006). Therefore, the differential accumulation

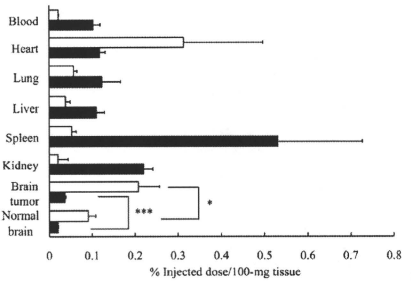

Fig. 6. Biodistribution of ^{18}F after injection of [^{18}F]SteP2-labeled PEG-liposomes or [^{18}F]-FDG. Injection of [^{18}F]SteP2-labeled liposomes and [^{18}F]-FDG was performed as described in the legend of Fig. 4. At 1 h after the injection, blood was collected; and the selected organs were then excised for the determination of the radioactivity. Data are presented as the mean distribution of ^{18}F after injection of [^{18}F]SteP2-labeled PEG-liposomes (closed bars, $n = 3$) or [^{18}F]FDG (open bars, $n = 4$). Significant differences between normal and tumor tissues are shown: $^{*}p < 0.05$, $^{***}p < 0.001$.

of PEG-liposomes and APRPG-liposomes observed in the tumor region, might be caused by the APRPG-modification of the latter liposomes.

In the present study HE-staining of normal brain tissue indicated that the capillaries were wrapped with astrocytes, whose arrangement may strengthen the BBB function (Standring, 2005). In contrast, astrocytes and nerve cells were not observed in the brain tumor tissues, and the capillaries directly faced the surrounding glioma cells: This might support the extravasation of PEG-liposomes into the tumor tissues. On the other hand, APRPG-liposomes might specifically accumulate in angiogenic vessels in brain tumor tissue. *Ex vivo* imaging of DiI with the *in vivo* fluorescence imaging system indicated the accumulation of both PEG-liposomes and APRPG-liposomes in the brain tumor was 3–4 fold higher than that in the surrounding normal brain tissue.

Our PET study indicated the accumulation of ^{18}F-labeled liposomes and imaging of glioma in the tumor-bearing rat brain. The tumor images obtained with liposomes were clearer than those obtained with FDG-PET. In the case of [^{18}F]FDG imaging, the background level represented by imaging of normal brain region was high, since persistent demand for glucose to normal brain cells (Fig. 5). In contrast, brain tumor was specifically imaged by using [^{18}F]-labeled PEG- or APRPG-liposomes with quite low background. Additionally, those liposomes also can be used for the brain cancer therapy.

The efficiency for tumor imaging by both [^{18}F]SteP2-labeled PEG-liposomes and APRPG-liposomes was similar, although the intratumoral distribution was different between PEG-liposomes and APRPG-liposomes. These data are consistent with our previous results showing that the accumulation of PEG-liposomes and APRPG-liposomes in solid tumors was not much different (Maeda et al., 2004). Therefore, we conclude that [^{18}F]-labeled liposomes having either passive or active targeting characteristics are useful for brain tumor imaging: However, active targeting liposomes to tumor angiogenic endothelium would be more potent when these are used for both imaging and therapy. In the present study, it should be also noted that a tumor with a diameter of only 1 mm could be successfully imaged by using [^{18}F]SteP2-labeled liposomes.

5. Conclusions

In the present study, brain tumor imaging by a DDS nanocarrier, i.e., liposomes, was explored. Liposomes were ^{18}F-labeled by the SophT method and injected intravenously into rats bearing a glioma-type brain tumor. Liposomes failed to accumulate in the normal surrounding brain tissue due to BBB protection and a brain tumor was specifically imaged with the liposomes via the different structure of brain tumor vessels. Since radiopharmaceutics or anticancer agents can be incorporated into DDS nanocarriers, these nanocarriers including liposomes should be useful for diagnosis and therapy of brain cancer.

References

Asai, T., Shimizu, K., Kondo, M., Kuromi, K., Watanabe, K., Ogino, K., Taki, T., Shuto, S., Matsuda, A., Oku, N., 2002. Anti-neovascular therapy by liposomal DPP-CNDAC targeted to angiogenic vessels. FEBS Lett. 520, 167–170.

Brastianos, P.K., Batchelor, T.T., 2009. VEGF inhibitors in brain tumors. Clin. Adv. Hematol. Oncol. 768, 753–760.

Chen, W., 2007. Clinical applications of PET in brain tumors. J. Nucl. Med. 48, 1468–1481.

Elbayoumi, T.A., Torchilin, V.P., 2006. Enhanced accumulation of long-circulating liposomes modified with the nucleosome-specific monoclonal antibody 2C5 in various tumours in mice: gamma-imaging studies. Eur. J. Nucl. Med. Mol. Imaging 33, 1196–1205.

Floeth, F.W., Pauleit, D., Sabel, M., Stoffels, G., Reifenberger, G., Riemenschneider, M.J., Jansen, P., Coenen, H.H., Steiger, H.J., Langen, K.J., 2007. Prognostic value of *O*-(2-^{18}Fluoroethyl)-L-tyrosine PET and MRI in low-grade glioma. J. Nucl. Med. 48, 519–527.

Gabizon, A.A., 2001. Pegylated liposomal doxorubicin: metamorphosis of an old drug into a new form of chemotherapy. Cancer Invest. 19, 424–436.

Geng, L., Osusky, K., Konjeti, S., Fu, A., Hallahan, D., 2004. Radiation-guided drug delivery to tumor blood vessels results in improved tumor growth delay. J. Control. Release 99, 369–381.

Hamoudeh, M., Kamleh, M.A., Diab, R., Fessi, H., 2008. Radionuclide delivery systems for nuclear imaging and radiotherapy of cancer. Adv. Drug Deliv. Rev. 60, 1329–1346.

Hatakeyama, T., Kawai, N., Nishiyama, Y., Yamamto, Y., Sasakawa, Y., Ichikawa, T., Tamiya, T., 2008. ^{11}C-methionine (MET) and ^{18}F-fluorothymidine (FLT) PET in patients with newly diagnosed glioma. Eur. J. Nucl. Med. Mol. Imaging 35, 2009–2017.

Heiss, P., Mayer, S., Herz, M., Wester, H.J., Schwaiger, M., Senekowitsch-Schmidtke, R., 1999. Investigation of transport mechanism and uptake kinetics of *O*-(2-[^{18}F]fluoroethyl)-L-tyrosine in vitro and in vivo. J. Nucl. Med. 40, 1367–1673.

Ishiwata, K., Kawamura, K., Wang, W.F., Furumoto, S., Kubota, K., Pascali, C., Bogni, A., Iwata, R., 2004. Evaluation of *O*-[^{11}C]methyl-L-tyrosine and *O*-[^{18}F]fluoromethyl-L-tyrosine as tumor imaging tracers by PET. Nucl. Med. Biol. 31, 191–198.

Jager, P.L., Vaalburg, W., Pruim, J., de Vries, E.G., Langen, K.J., Piers, D.A., 2001. Radiolabeled amino acids: basic aspects and clinical applications in oncology. J. Nucl. Med. 42, 432–445.

Kato, T., Shinoda, J., Nakayama, N., Miwa, K., Okumura, A., Yano, H., Yoshimura, S., Maruyama, T., Muragaki, Y., Iwama, T., 2008. Metabolic assessment of gliomas using ^{11}C-methionine, [^{18}F] fluorodeoxyglucose, and ^{11}C-choline positron-emission tomography. AJNR Am. J. Neuroradiol. 29, 1176–1182.

Kondo, M., Asai, T., Katanasaka, Y., Sadzuka, Y., Tsukada, H., Ogino, K., Taki, T., Baba, K., Oku, N., 2004. Anti-neovascular therapy by liposomal drug targeted to membrane type-1 matrix metalloproteinase. Int. J. Cancer 108, 301–306.

Kostarelos, K., Emfietzoglou, D., 2000. Tissue dosimetry of liposome–radionuclide complexes for internal radiotherapy: toward liposome-targeted therapeutic radiopharmaceuticals. Anticancer Res. 20, 3339–3345.

Langen, K.J., Hamacher, K., Weckesser, M., Floeth, F., Stoffels, G., Bauer, D., Coenen, H.H., Pauleit, D., 2006. *O*-(2-[^{18}F]fluoroethyl)-L-tyrosine: uptake mechanisms and clinical applications. Nucl. Med. Biol. 33, 287–294.

Maeda, H., Wu, J., Saw, T., Matsumura, Y., Hori, K., 2000. Tumor vascular permeability and the EPR effect in macromolecular therapeutics: a review. J. Control. Release 65, 271–284.

Maeda, H., Bharate, G.Y., Daruwalla, J., 2009. Polymeric drugs for efficient tumor-targeted drug delivery based on EPR-effect. Eur. J. Pharm. Biopharm. 71, 409–419.

Maeda, N., Takeuchi, Y., Takada, M., Sadzuka, Y., Namba, Y., Oku, N., 2004. Anti-neovascular therapy by use of tumor neovasculature-targeted long-circulating liposome. J. Control. Release 100, 41–52.

Maeda, N., Miyazawa, S., Shimizu, K., Asai, T., Yonezawa, S., Kitazawa, S., Namba, Y., Tsukada, H., Oku, N., 2006. Enhancement of anticancer activity in antineovascular therapy is based on the intratumoral distribution of the active targeting carrier for anticancer drugs. Biol. Pharm. Bull. 29, 1936–1940.

Mehrkens, J.H., Pöpperl, G., Rachinger, W., Herms, J., Seelos, K., Tatsch, K., Tonn, J.C., Kreth, F.W., 2008. The positive predictive value of *O*-(2-[^{18}F]fluoroethyl)-

L-tyrosine (FET) PET in the diagnosis of a glioma recurrence after multimodal treatment. J. Neurooncol. 88, 27–35.
Nakamoto, Y., Togashi, K., Kaneta, T., Fukuda, H., Nakajima, K., Kitajima, K., Murakami, K., Fujii, H., Satake, M., Tateishi, U., Kubota, K., Senda, M., 2009. Clinical value of whole-body FDG-PET for recurrent gastric cancer: a multicenter study. Jpn. J. Clin. Oncol. 39, 297–302.
Nojiri, T., Nariai, T., Aoyagi, M., Senda, M., Ishii, K., Ishiwata, K., Ohno, K., 2009. Contributions of biological tumor parameters to the incorporation rate of L-[methyl-^{11}C] methionine into astrocytomas and oligodendrogliomas. J. Neurooncol. 93, 233–241.
Oku, N., Tokudome, Y., Tsukada, H., Kosugi, T., Namba, Y., Okada, S., 1996. In vivo trafficking of long-circulating liposomes in tumour-bearing mice determined by positron emission tomography. Biopharm. Drug Dispos. 17, 435–441.
Oku, N., Asai, T., Watanabe, K., Kuromi, K., Nagatsuka, M., Kurohane, K., Kikkawa, H., Ogino, K., Tanaka, M., Ishikawa, D., Tsukada, H., Momose, M., Nakayama, J., Taki, T., 2002. Anti-neovascular therapy using novel peptides homing to angiogenic vessels. Oncogene 21, 2662–2669.
Pauleit, D., Stoffels, G., Bachofner, A., Floeth, F.W., Sabel, M., Herzog, H., Tellmann, L., Jansen, P., Reifenberger, G., Hamacher, K., Coenen, H.H., Langen, K.J., 2009. Comparison of ^{18}F-FET and ^{18}F-FDG PET in brain tumors. Nucl. Med. Biol. 36, 779–787.
Sakakibara, T., Chen, F.A., Kida, H., Kunieda, K., Cuenca, R.E., Martin, F.J., Bankert, R.B., 1996. Doxorubicin encapsulated in sterically stabilized liposomes is superior to free drug or drug-containing conventional liposomes at suppressing growth and metastases of human lung tumor xenografts. Cancer Res. 56, 3743–3746.
Scott, A.M., Gunawardana, D.H., Bartholomeusz, D., Ramshaw, J.E., Lin, P., 2008. PET changes management and improves prognostic stratification in patients with head and neck cancer: results of a multicenter prospective study. J. Nucl. Med. 49, 1593–1600.
Standring, S., 2005. GRAY'S Anatomy, 39th ed. Elsevier, Edinburgh, pp. 51–52.
Syme, A.M., McQuarrie, S.A., Middleton, J.W., Fallone, B.G., 2003. Dosimetric model for intraperitoneal targeted liposomal radioimmunotherapy of ovarian cancer micrometastases. Phys. Med. Biol. 48, 1305–1320.
Takeda, A., Tamano, H., Oku, N., 2003. Alteration of zinc concentrations in the brain implanted with C6 glioma. Brain Res. 965, 170–173.
Tang, G., Wang, M., Tang, X., Luo, L., Gan, M., 2003. Synthesis and evaluation of O-(3-[18F]fluoropropyl)-L-tyrosine as an oncologic PET tracer. Nucl. Med. Biol. 30, 733–739.
Tian, M., Zhang, H., Oriuchi, N., Higuchi, T., Endo, K., 2004. Comparison of ^{11}C-choline PET and FDG PET for the differential diagnosis of malignant tumors. Eur. J. Nucl. Med. Mol. Imaging 31, 1064–1172.
Ullrich, R.T., Kracht, L., Brunn, A., Herholz, K., Frommolt, P., Miletic, H., Deckert, M., Heiss, W.D., Jacobs, A.H., 2009. Methyl-L-^{11}C-methionine PET as a diagnostic marker for malignant progression in patients with glioma. J. Nucl. Med. 50, 1962–1968.
Urakami, T., Akai, S., Katayama, Y., Harada, N., Tsukada, H., Oku, N., 2007. Novel amphiphilic probes for [^{18}F]-radiolabeling preformed liposomes and determination of liposomal trafficking by positron emission tomography. J. Med. Chem. 50, 6454–6457.
Urakami, T., Sakai, K., Asai, T., Fukumoto, D., Tsukada, H., Oku, N., 2009. Evaluation of *O*-[^{18}F]fluoromethyl-D-tyrosine as a radiotracer for tumor imaging with positron emission tomography. Nucl. Med. Biol. 36, 295–303.
Verhoeff, J.J., Stalpers, L.J., Claes, A., Hovinga, K.E., Musters, G.D., Vandertop, W.P., Richel, D.J., Leenders, W.P., van Furth, W.R., 2009. Tumour control by whole brain irradiation of anti-VEGF-treated mice bearing intracerebral glioma. Eur. J. Cancer 45, 3074–3080.
Wen, P.Y., Kesari, S., 2008. Malignant gliomas in adults. N. Engl. J. Med. 359, 492–507.
Yamamoto, Y., Nishiyama, Y., Kimura, N., Kameyama, R., Kawai, N., Hatakeyama, T., Kaji, M., Ohkawa, M., 2008. ^{11}C-acetate PET in the evaluation of brain glioma: comparison with ^{11}C-methionine and ^{18}F-FDG-PET. Mol. Imaging Biol. 10, 281–287.

uicc
global cancer control

IJC
International Journal of Cancer

Cancer antineovascular therapy with liposome drug delivery systems targeted to BiP/GRP78

Yasufumi Katanasaka[1,2,3], Takayuki Ishii[1,2], Tomohiro Asai[1,2], Hirotaka Naitou[2,4], Noriyuki Maeda[5], Fumiaki Koizumi[3], Shinichi Miyagawa[6], Norio Ohashi[2,7] and Naoto Oku[1,2]

[1] Department of Medical Biochemistry, Graduate School of Pharmaceutical Sciences, University of Shizuoka, Suruga-ku, Shizuoka, Japan
[2] Global COE Program, University of Shizuoka, Suruga-ku, Shizuoka, Japan
[3] Shien-Lab, National Cancer Center Hospital, Chuo-ku, Tokyo, Japan
[4] Laboratory of Environmental Microbiology, Institute for Environmental Sciences, University of Shizuoka, Shizuoka, Japan
[5] Nippon Fine Chemical., Ltd., Takasago, Hyogo, Japan
[6] Department of Surgery, Shinshu University School of Medicine, Matsumoto, Nagano, Japan
[7] Laboratory of Microbiology, Graduate School of Nutritional and Environmental Sciences, University of Shizuoka, Shizuoka, Japan

Angiogenesis is crucial for tumor growth and hematogenous metastasis. Specifically expressed and functional protein molecules in angiogenic endothelial cells, especially on the plasma membrane, may be molecular targets for antiangiogenic drugs and drug delivery systems (DDS) in cancer therapy. To discover such target molecules, we performed subcellular proteome analysis of human umbilical vein endothelial cells (HUVECs) treated with or without vascular endothelial growth factor (VEGF) using 2-dimensional difference in-gel electrophoresis (2D-DIGE) and matrix-assisted laser desorption/ionization tandem time-of-flight mass spectrometry (MALDI-TOF/TOF-MS). Among the identified proteins, BiP/GRP78, a molecular chaperone, was highly expressed in the membrane/organelle fraction of HUVECs after VEGF treatment. The involvement of BiP in VEGF-induced angiogenesis was examined by RNA interference. BiP knockdown significantly suppressed VEGF-induced endothelial cell proliferation and VEGF-induced phosphorylation of extracellular-regulated kinase 1/2, phospholipase C-γ, and VEGF receptor-2 in HUVECs. Cell surface biotinylation analysis revealed that the cell surface expression of BiP was elevated in VEGF-activated HUVECs. Aiming to apply BiP to a target molecule in liposomal DDS, we developed liposomes modified with the WIFPWIQL peptide, which has been shown to bind to BiP, and investigated its potential for cancer therapy. The WIFPWIQL-modified liposomes (WIFPWIQL liposomes) were significantly taken up by VEGF-activated HUVECs as compared to peptide-unmodified liposomes. WIFPWIQL liposomes appeared to accumulate in tumor endothelial cells *in vivo*. WIFPWIQL liposomes containing doxorubicin significantly suppressed tumor growth and prolonged the survival of colon26 NL-17 carcinoma cell-bearing mice. In summary, BiP may regulate VEGF-induced endothelial cell proliferation through VEGFR-2-mediated signaling and be an effective target molecule for cancer antineovascular therapy.

Angiogenesis, the process of sprouting new blood vessels from preexisting vessels, is critical for tumor growth and blood-borne metastasis.[1] The overall process of angiogenesis is regulated by the balance between proangiogenic and anti-angiogenic factors secreted from several cell types in a tumor microenvironment, such as tumor cells, fibroblasts and macrophages.[2,3] Endothelial cells in tumors differentially express various protein molecules compared to those in normal tissues.[4] In intratumoral regions, under hypoxic conditions, tumor cells produce vascular endothelial growth factor

Key words: BiP/GRP78, antineovascular therapy, drug delivery systems, subcellular proteomics, tumor angiogenesis

Abbreviations: 2D-DIGE: 2-dimensional difference in-gel electrophoresis; BiP: immunoglobulin heavy-chain binding protein; DDS: drug delivery systems; DSPC: distearoylphosphatidylcholine; DSPG: distearoylphosphatidylglycerol; DSPE-PEG: distearoylphosphatidylethanolamine conjugated polyethyleneglycol 2000; DOX: doxorubicin; EBM-2: endothelial basal medium-2; EGM-2: endothelial growth medium-2; ER: endoplasmic reticulum; ERK: extracellular-regulated kinase; FBS: fetal bovine serum; GFP: green fluorescent protein; GRP78: glucose-regulated protein 78 kDa; HUVECs: human umbilical vein endothelial cells; MALDI-TOF/TOF-MS: matrix-assisted laser desorption/ionization tandem time of flight mass spectrometry; MAPK: mitogen-activated protein kinase; PEG-Lip-DOX: PEG-liposomal DOX; PLCγ: phospholipase C-γ; RNAi: RNA interference; siRNA: small interfering RNA; VEGF: vascular endothelial growth factor; WIFPWIQL liposomes: WIFPWIQL peptide-modified liposomes; WIFPWIQL-Lip-DOX: WIFPWIQL-liposomal DOX

Grant sponsor: Japanese Ministry of Education, Culture, Sports, Science and Technology
DOI: 10.1002/ijc.25276
History: Received 11 Sep 2009; Accepted 25 Jan 2010; Online 22 Feb 2010

Correspondence to: Naoto Oku, Department of Medical Biochemistry, University of Shizuoka, 52-1 Yada, Suruga-ku, Shizuoka 422-8526, Japan, Tel.: +81-54-264-5701, Fax: +81-54-264-5705, E-mail: oku@u-shizuoka-ken.ac.jp

(VEGF), a principal proangiogenic factor, through hypoxia-inducible factor 1-dependent transcription.[5] VEGF and its receptor (VEGFR) have been well studied in basic and clinical cancer research, and inhibitors of VEGF signal transduction have been developed as anticancer drugs.[6] The activation of VEGFRs initiates the proliferation, migration and invasion of endothelial cells. VEGF induces the phosphorylation of VEGFR tyrosine kinases, and thereby activates mitogen-activated protein kinase (MAPK) mediated by phospholipase C-γ (PLCγ) or the AKT/PKB signal cascade mediated by phosphatidylinositol-3 kinase (PI3K).[7]

Comparative proteome analysis is a powerful tool to find differentially expressed proteins[8,9]; and it is rendered more powerful by combining it with subcellular fractionation, whereby it can identify low-abundance proteins in cellular organelles by subtracting out common protein contaminants.[10,11] The proteins on the plasma membrane play a role in fundamental cellular processes, including ion and solute transports, signal transduction or cell adhesion. Since alterations in the expression of membrane proteins are often related to diseases, such proteins may become molecular targets for diagnostic and therapeutic approaches.[12–14] Comprehensive profiling of these proteins may also provide a better understanding of how a cell responds to a variety of intracellular and extracellular signals. Therefore, expression profiling of membrane proteins in specific cell types under defined conditions has become a central point of many molecular biology investigations.

Inhibition of angiogenesis has curative benefits such as inhibition of primary tumor growth as well as suppression of blood-borne metastasis.[15] Therapeutic vascular targeting has been categorized into antiangiogenic approaches, which aim to prevent the neovascularization processes in tumors, whereas vascular-disrupting approaches—using vascular disrupting agents—aim to damage the established tumor vasculature.[16] Antineovascular therapy is a strategy targeted against angiogenic neovasculature by using liposome drug delivery systems (DDS).[17–19] We and other groups have previously reported that tumor vasculature-targeted liposomes can deliver encapsulated agents to angiogenic endothelial cells and have demonstrated their therapeutic advantages.[20,21] Cell surface proteins specifically expressed in angiogenic endothelial cells are possible molecular targets for DDS because these cells are in direct contact with the blood stream, making it easy for drug carriers to recognize them after modifying these carriers with appropriate targeting tools such as antibodies, peptides or carbohydrates. However, it appears that there are few target molecules for tumor vasculature-targeted drug delivery, and the identification of novel target molecules would contribute to the development of DDS in cancer therapeutics.

Here, we describe subcellular proteome analysis of human umbilical vein endothelial cells (HUVECs) treated with or without VEGF to discover the target molecules expressed on the cellular membranes of angiogenic endothelial cells using 2-dimensional difference in-gel electrophoresis (2D-DIGE) and matrix-assisted laser desorption/ionization tandem time-of-flight mass spectrometry (MALDI-TOF/TOF-MS); and then describe the functional analysis of BiP (immunoglobulin heavy chain-binding protein), which is also called glucose-regulated protein 78 kDa (GRP78) and is an identified protein in the proteomic analysis. Moreover, we developed BiP-targeted liposomes and evaluated the utility of BiP-targeted drug delivery in cancer antineovascular therapy.

Material and Methods

Cell culture

HUVECs (Cambrex Corporation, Walkersville, MD) were maintained in endothelial growth medium-2 (EGM-2, Cambrex Corporation) at 37°C under 5% CO_2 in a humidified chamber, as described previously.[17] HUVECs were used at passage 7 or less in all the experiments. Mouse colon26 NL-17 carcinoma cells (C26) and human prostate carcinoma DU145 cells were cultured in an appropriate medium supplemented with streptomycin (100 μg/mL), penicillin (100 units/mL) and 10% heat-inactivated fetal bovine serum (FBS) at 37°C in 5% CO_2.

Cellular protein fractionation

HUVECs were grown to subconfluence (80–90% confluence) in T-150 flasks, and the culture medium was replaced with 0.5% FBS-containing endothelial basal medium-2 (EBM-2, Cambrex Corporation). After serum starvation by overnight incubation, recombinant human $VEGF_{165}$ (rhVEGF, 20 ng/mL as final concentration; BD Biosciences, San Diego, CA) was added to the starved cells, which were then further incubated for 24 hr at 37°C. The cells were washed with ice-cold PBS (pH 7.4), and the proteins in the membrane/organelle were separately extracted using a Subcellular Proteome Extraction Kit (Calbiochem, San Diego, CA) according to the manufacturer's recommended protocol. The proteins in each fraction were precipitated using a Protein Precipitant Kit (Calbiochem) to concentrate the proteins and to remove interfering substances according to the manufacturer's recommended protocol. The precipitated proteins were then resolubilized in lysis buffer for 2D-DIGE (7 M urea, 2 M thiourea, 4% CHAPS, 30 mM Tris-HCl; pH 8.5), and the protein concentration was determined by the Bradford protein assay method (Bio-Rad Laboratories, Tokyo, Japan).

2D-DIGE

2D-DIGE was performed as previously described,[22] and reagents used for 2D-DIGE were purchased from GE Healthcare UK (Buckinghamshire, UK). An internal standard was prepared by pooling an equal amount of each protein from VEGF-stimulated and nonstimulated HUVECs. Then, 50 μg of protein from the internal standard, nontreated sample and VEGF-stimulated sample was fluorescence-labeled with 400 pmol of Cy2, Cy3 and Cy5, respectively, on ice for 30 min in the dark. The labeling reaction was quenched with 10 mM L-lysine. The fluorescently labeled samples were mixed and

adjusted to a final volume of 450 μL with rehydration buffer (7 M urea, 2 M thiourea, 2% CHAPS, 1% DTT and 0.002% bromophenol blue). The samples were applied to isoelectric focusing polyacrylamide gel electrophoresis (IEF) using IPG strips (pH 3–10, nonlinear, 24 cm) and IPGphor II. The IPG strips were rehydrated with CyDye-labeled samples at 20°C for 12 hr, and IEF was performed in IPGphor at 20°C with a total of 80 kVh. The IPG strips were equilibrated for 15 min by shaking gently in an equilibration buffer (6 M urea, 30% glycerol, 2% SDS, 1.5 M Tris-HCl; pH 8.8) containing DTT (10 mg/mL) and then for 15 min in an equilibration buffer containing iodoacetoamide (25 mg/mL) instead of DTT. The equilibrated IPG strips were transferred onto 10% polyacrylamide gels and 2D electrophoresis was performed using the Ettan Dalt II system. The 2D-gel images were scanned at appropriate wavelengths for Cy2, Cy3 and Cy5 dyes with a Typhoon 9400™ scanner; and the spot volumes were analyzed quantitatively using the biological variation analysis (BVA) mode of DyCyder software (version 5.0). Spots of interest were defined from average ratios of VEGF-stimulated over nonstimulated, which were above 1.5 or below −1.5-fold (0.67-fold) with significant difference (4 separate gels, Student's *t*-test, $p < 0.05$).[23]

Mass spectrometry and protein identification

For mass spectrometry analysis, 500 μg of the pooled proteins was applied to 2D electrophoresis and then stained with Deep Purple, according to the manufacturer's instructions. The gel was imaged with a Typhoon 9400 scanner. The matched spots of interest were picked with Ettan Spot Picker. In-gel digestion was performed as follows. The gel pieces picked were destained with 50 mM NH_4HCO_3 in 50% acetonitrile (ACN) and dehydrated with 100% ACN. The dried gel pieces were added to trypsin solution (25 ng/mL, Promega, Madison, WI) and incubated overnight at 37°C. The digested peptides were extracted with 1% trifluoroacetic acid (TFA) in 80% ACN and concentrated with a vacuum centrifuge. The peptide solutions were desalted and concentrated with ZipTip C18μ (Millipore, Bedford, MA). Then, the peptide solutions were mixed with α-cyano-4-hydroxycinnamic acid (Sigma, Tokyo, Japan) and applied onto a target plate (Bruker Daltonics, Bremen, Germany). The MS and MS/MS spectra were obtained using an Ultraflex mass spectrometer (Bruker Daltonics) in the reflector mode. The acquired spectra were analyzed using Flexanalysis software (version 2.2, Bruker Daltonics) in the default mode. The protein species were identified by peptide mass fingerprinting and/or combined search using Biotool software (version 2.2, Bruker Daltonics) of the Mascot search engine (version 2.0, Matrix Science, London, UK) against the NCBI database.

Western blot analysis

Western blotting was performed as described previously[24] with some modifications. The cells were washed with ice-cold PBS and lysed with 10 mM Tris-HCl (pH 7.4) containing 0.1% SDS, 2 mM phenylmethylsulfonyl fluoride (PMSF), 50 μg/mL aprotinin, 200 μM leupeptin and 100 μM pepstatin A. To examine the phosphorylation of VEGFR-2, PLCγ and ERK1/2, we stimulated starved HUVECs with rhVEGF for 5 or 10 min. The protein concentration was determined by using the BCA protein assay kit (Pierce, Tokyo, Japan). The protein samples were mixed with SDS-PAGE sample buffer (2% SDS, 10% glycerol, 6% 2-mercaptoethanol, 50 mM Tris-HCl; pH 6.8), and an equal amount of proteins in each sample was subjected to SDS-PAGE. The separated proteins were transferred to a PVDF membrane (Millipore) and blocked with 5% skim-milk in TBST (0.9% NaCl, 0.1% Tween20, 20 mM Tris-HCl; pH7.4). The primary antibodies used were anti-GRP78 (BiP) antibody (Santa Cruz Biotechnology, San Diego, CA), antiactin antibody (Sigma), anti-GAPDH antibody (Abcam, Cambridge, UK), antiphospho-ERK1/2 (Thr183/Tyr185), anti-ERK1/2 (Promega), antiphospho-PLCγ1 (Tyr783), anti-PLCγ1, antiphospho-VEGFR-2 (Tyr1175) and anti-VEGFR-2 (Cell Signaling Technology, Beverly, MA). Horseradish peroxidase (HRP)-conjugated antibodies were used as secondary antibodies. The PVDF membrane was developed with ECL reagent (GE Healthcare). The band density was measured with ImageJ software.

Cell-surface biotinylation

Extraction of cell-surface proteins was performed with a Cell Surface Biotinylation Kit (Pierce) according to the manufacturer's instructions. In brief, HUVECs were washed with ice-cold PBS, treated with NHS-SS-Biotin, and further incubated at 4°C for 30 min to conjugate the cell-surface proteins with NHS-SS-Biotin. After quenching the protein-NHS reaction, the cells were scraped and centrifuged at 500*g* for 3 min at 4°C. The cell pellets were then solubilized by sonication in the manufacturer's supplied lysis buffer and centrifuged at 10,000*g* for 3 min at 4°C. The protein samples in the supernatant were applied to a NeutrAvidin™ column and the biotin-conjugated cell-surface proteins were eluted with 50 mM DTT-containing buffer (0.1% SDS, 62.5 mM Tris-HCl; pH 6.8).

RNA interference

RNA interference (RNAi) was performed with DharmaFECT™ reagent (GE Healthcare) according to the manufacturer's instructions. HUVECs were seeded at 2.0×10^5 cells (80–90% confluence) in an antibiotic-free EGM-2 medium and incubated overnight. The cells were transfected with 100 nM of small interfering RNA (siRNA, Hokkaido System Sciences, Hokkaido, Japan) using DharmaFECT™ reagent. The sequences of siRNA for BiP (BiP siRNA) were 5′-GGU UAC CCA UGC AGU UGU UTT-3′ (sense) and 5′-AAC AAC UGC AUG GGU AAC CTT-3′ (antisense), as previously described.[25] The sequences of siRNA for green fluorescent protein (GFP siRNA used as nonsilencing control siRNA) have been described previously.[26] After incubation with these siRNAs for 48 hr at 37°C, the effects of each siRNA on

protein expression were determined by Western blot analysis and real-time PCR.

RNA isolation and real-time PCR

Total RNA was isolated using ISOGEN (Nippon Gene, Tokyo, Japan) and the resulting RNA was reverse transcribed. TaqMan real-time PCR assay was performed using TaqMan gene expression assays on a StepOnePlus (Applied Biosystems, Tokyo, Japan). The relative real-time PCR quantification was based on a comparative quantitation method. The endogenous reference gene was GAPDH. The specificity of the PCR reactions was confirmed by a single band of the predicted size after agarose gel electrophoresis (data not shown).

Cell proliferation assay

HUVECs were transfected with each siRNA as described above and incubated for 24 hr at 37°C. The transfected cells were harvested and reseeded at 2.0×10^4 cells per well on a 24-well plate in 0.5% FBS-containing EBM-2 medium with or without rhVEGF (20 ng/mL). The cells were further incubated for 24 or 48 hr, and the cell viability was determined at each time with TetraColor One™ (Seikagaku, Tokyo, Japan). The growth ratio was calculated by the absorbance (450 nm) at 24 hr/3 hr and 48 hr/3 hr. The absorbance at 3 hr was considered to reflect the cell number immediately after seeding the cells without cell proliferation.

Preparation of liposomes

Distearoyl phosphatidylcholine (DSPC), distearoyl phosphatidylglycerol (DSPG), cholesterol and distearoyl phosphatidylethanolamine-conjugated polyethyleneglycol 2000 (DSPE-PEG) or the DSPE-PEG conjugate of GWIFPWIQL-peptides, which are shown to bind to BiP/GRP78,[27] were dissolved in tert-butylalcohol (10:10:10:1 as a molar ratio). The lipid solutions were lyophilized, and the lyophilizates were hydrated with 0.3 M sucrose solution (pH 7.4). The liposome solutions were frozen and thawed for 3 cycles with liquid nitrogen. Then, the liposome size was adjusted by extruding through polycarbonate filters of 100-nm pore size (Nuclepore, Cambridge, MA). For the preparation of doxorubicin (DOX)-containing liposomes, DOX solutions were added to the initial lipid solutions in the proportion of 30 mol % to the composed lipids (DSPC + DSPG). Unencapsulated DOX was removed by ultracentrifugation at 604,000*g* for 15 min (HITACHI, Tokyo, Japan), and the amount of DOX in the liposome was determined by measuring the absorbance at 484 nm. The liposome size was measured using ZETASIZER (Malvern Instruments, Malvern, UK).

Cellular uptake of liposomes

The liposomes were radiolabeled by adding [^{3}H]cholesteryl hexadecyl ether solution (370 kBq/mL, GE Healthcare) to the initial lipid solution. HUVECs were seeded (2.0×10^5 cells) on a 35-mm dish and stimulated with rhVEGF as described above. C26 or DU145 cells (both 1.0×10^5 cells) were also seeded on a 35-mm dish and incubated overnight. The radiolabeled liposomes were added to the cells and further incubated for 2 hr. The cells were washed with PBS and solubilized with 10 mM Tris-HCl buffer containing 0.1% SDS (pH 7.4). The cell lysates were recovered and transferred to HionicFluor (Perkin Elmer, Foster City, CA). Radioactivity was determined with a liquid scintillation counter (LSC-3500; Aloka, Tokyo, Japan).

Intratumoral distribution of WIFPWIQL liposomes

The liposomes were fluorescently labeled by adding DiI C18 (Molecular Probes, Eugene, OR) solution to the initial lipid solution. C26 cells were subcutaneously implanted into the posterior flank of 5-week-old BALB/c male mice. The DiI C18-labeled liposomes were intravenously injected into the mice 10 days after tumor implantation. At 3 or 6 hr after injection of the liposomes, the mice were sacrificed using diethyl ether anesthesia, and the tumors were dissected. Immunostaining was performed as described previously. The tumor tissues were embedded and frozen with dry ice/ethanol. Tumor sections (10 μm) were prepared with cryostatic microtome (HM 505E; Microm, Walldorf, Germany) and air-dried for at least 1 hr. The sections were incubated in 1% bovine serum albumin containing PBS for 10 min at room temperature for protein blocking, with biotinylated anti-mouse CD31 rat monoclonal antibody (BD Pharmingen, Franklin Lakes, NJ) for 18 hr at 4°C, and then with streptavidin-Alexa Fluor 488 conjugates (Molecular Probes) for 30 min at room temperature. Finally, the sections were mounted with Perma Fluor Aqueous Mounting Medium (Thermo Shandon, Pittsburgh, PA) and fluorescently observed with a microscopic LSM system (Carl Zeiss, Germany).

Dorsal air sac model

Dorsal air sac model mice were prepared as follows: C26 cells (1.0×10^7 cells/150 μL) were loaded into a chamber ring (Millipore) covered with filters (0.45-nm pore size, Millipore). The chamber ring was then implanted subcutaneously into the dorsal skin of the mice. At days 2 and 3, 0.3 M sucrose solution (control), PEG-liposomal doxorubicin (PEG-Lip-DOX) or WIFPWIQL-liposomal doxorubicin (WIFPWIQL-Lip-DOX) was intravenously administered (5 mg/kg/day as dose of DOX). At day 4, the mice were sacrificed using diethyl ether and the dorsal skin osculating the chamber ring was observed.

Therapeutic experiment

PEG-Lip-DOX, WIFPWIQL-Lip-DOX (5 mg/kg/day as dose of DOX) or 0.3 M sucrose solution (control) was intravenously administered to the C26-bearing mice at days 6, 9, 12 and 15 after tumor implantation. The tumor size and body weight of each mouse were monitored. The animals used in the experiments were cared for according to the guidelines for the care and use of laboratory animals of the University of Shizuoka.

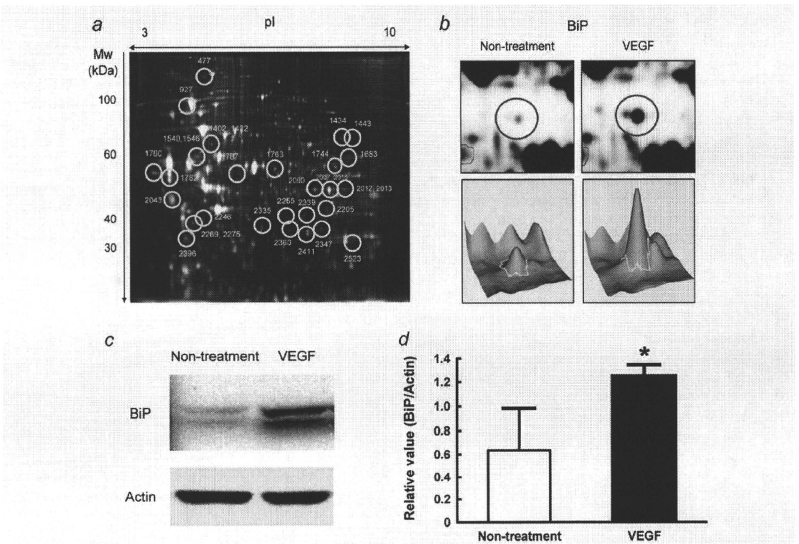

Figure 1. 2D-DIGE analysis of protein expression in the membrane/organelle from nontreated and VEGF-stimulated HUVECs. HUVECs were stimulated with or without rhVEGF (20 ng/mL) for 24 hr. Then, proteins in membrane/organelle fractions were extracted and fluorescently labeled with Cy2 (internal standard), Cy3 (nontreatment) and Cy5 (VEGF-treatment). The protein samples were applied onto 4 separate gels and were 2-dimensionally electrophoresed. (*a*) The 2D-gel images of membrane/organelle fraction were scanned with a Typhoon 9400 scanner. Red spots show increased expression and green spots show decreased expression after VEGF-treatment. The master numbers correspond to those in Table 1. (*b*) The gel and 3D images of the protein spot identified as BiP by mass spectrometry are also shown. (*c*, *d*) Western blot analysis against BiP was performed. Whole cell lysates were collected; Western blotting was performed and the relative band density (BiP/Actin) was determined. The bars indicate the mean ± SD ($n = 3$), $^*p < 0.05$. Similar results were obtained in a separate experiment.

Protein extraction from cancer patients

Tumor specimens were obtained from 11 patients (8 men and 3 women; mean age 61.8; range, 35–77 years) who had undergone surgery for colon cancer at the Department of Surgery, Shinshu University Hospital from September 2005 to March 2006. Informed consent was obtained from each patient and the study was conducted after Human Experimentation Review by the institutional committee. The tissues were homogenized and the protein samples were subjected to Western blot analysis as described above.

Statistical analysis

All experiments in our study were repeated twice or more. Significant differences were analyzed by unpaired Student's *t*-test or analysis of variance (ANOVA) with Tukey's *post-hoc* test. Survival analysis was performed with log-rank test. A value of $p < 0.05$ was considered to be statistically significant.

Results

Subcellular proteome analysis of membrane/organelle fraction prepared from HUVECs stimulated with VEGF

To identify the specifically expressed proteins in angiogenic endothelial cells, we performed a subcellular fractionation of membranes/organelles, and then analyzed the protein expression profiles between VEGF-stimulated and nonstimulated HUVECs by 2D-DIGE. Of approximately 2,500 protein spots detected on the 2D-gels, we successfully identified 36 spots in the membrane/organelle fraction by MALDI-TOF/TOF-MS (Fig. 1*a* and Table 1). Among them, the expression of BiP was remarkably increased after VEGF stimulation (Fig. 1*b*). We examined the change in BiP expression levels due to

Table 1. Differentially expressed proteins of VEGF-stimulated HUVECs

Definition	Master number[1]	NCBI accession number	Average ratio[2]	M_w[3]	pI[3]	Number of peptides[4]	Mascot score	Coverage %[5]	Identified peptides[6]	Ion score
Acetyl CoA transferase-like protein	2339	19880019	1.61	41,225	6.27	7/66	97	17	AGHFDKEIVPVLVSTR	32
BiP protein	1402	6470150	1.82	70,888	5.23	10/81	73	21		
	1422	6470150	3.34	70,388	5.23	12/61	117	24		
	1787	6470150	2.17	70,388	5.23	17/72	143	28	VTHAWTVPAYFNDAQR	44
Calponin 3	2335	4502923	1.59	36,391	5.69	9/77	86	35		
Calreticulin	1782	30583735	−1.52	48,112	4.29	8/77	128	26	EQFLDGDGWTSR	59
Calumenin	2043	2809324	−1.61	37,050	4.47	21/58	234	59	WIYEDVER	62
Chain B, A sort peptide insertion crucial for angiostatic of human tryptophanyl-tRNA synthetase	1763	42543731	1.51	44,706	6.41	16/82	223	57	KPFYLYTGR	47
Chain D, structure of the human Mcad: eff complex	2205	49259284	1.58	43,615	7.01	10/63	133	28	IYQIYEGTSQIQR	42
EEF2 protein	2360	33869643	2.5	64,739	8.77	10/63	113	25		
EGF-containing fibulin-like extracellular matrix protein 1 isoform b	1546	9665253	1.9	54,604	4.95	16/79	141	46		
ENO1 protein	2000	29792061	1.53	47,139	7.01	12/59	229	40	AAVPSGASTGIYEALELR	159
	2007	29792061	1.52	47,139	7.01	16/65	275	48	AAVPSGASTGIYEALELR	160
	2012	29792061	1.6	47,139	7.01	12/84	149	40	AAVPSGASTGIYEALELR	80
	2013	29792061	1.56	47,139	7.01	8/62	102	26	AAVPSGASTGIYEALELR	32
	2016	29792061	1.76	47,139	7.01	16/72	235	51	AAVPSGASTGIYEALELR	124
Leucine-zipper protein FKSG13	1760	11034809	−2.33	43,449	5.67	7/65	215	23	IIGAVDQIQLTQAQLEER	116
									VPPFTFHVK	37
N-acetylneuraminic acid phosphate synthase	2347	12056473	1.67	40,281	6.29	9/68	158	37	PLELELCPGR	67
Oxygen-regulated protein precursor	477	5453832	1.92	111,266	5.16	16/84	99	19		
Protein disulfide isomerase-related protein 5	2255	1710248	3.18	46,170	4.95	12/64	94	43		
PRPF4	1683	48146327	1.97	58,270	7.05	11/85	92	30		
Pyruvate kinase3, isofrom 1	1683	31416989	1.97	57,942	7.96	10/86	81	27		
TKT protein	1434	31417921	1.52	49,879	8.02	8/70	101	28		
	1443	31417921	1.68	49,879	8.02	8/61	108	24	VLDPFTIKPLDR	39
Heat shock protein gp96 precursor	2246	15010550	2.17	90,138	4.73	11/67	105	16	LGVIEDHSNR	33
	2269	15010550	2.85	90,138	4.73	16/58	97	19		
	2275	15010550	2.17	90,138	4.73	17/44	119	22		

Table 1. Differentially expressed proteins of VEGF-stimulated HUVECs (Continued)

Definition	Master number[1]	NCBI accession number	Average ratio[2]	M_w[3]	pI[3]	Number of peptides[4]	Mascot score	Coverage %[5]	Identified peptides[6]	Ion score
	2396	15010550	2.56	90,138	4.73	16/59	140	21	IYFMAGSSR	39
Tumor rejection antigen (gp96) 1	927	4507677	1.86	90,411	4.76	33/53	198	50	FAFQAEVNR	43
	1540	4507677	1.92	92,411	4.76	12/58	134	21		
	1546	4507677	1.9	92,411	4.76	11/84	103	18	FAFQAEVNR	34
UDP-galactose 4′ pimerase	2411	2947219	1.59	38,285	6.26	7/72	82	24		
UDP-glucose dehydrogenase	1744	4507813	1.82	54,989	6.73	22/78	268	65	AVQALCAVYEHWVPR	22
Unknown	1540	62822120	1.92	36,095	5.03	8/62	73	34		
Valosin-containing protein	2523	11095436	1.84	34,870	6.08	11/74	86	43		

[1]Master number is the unique number of the position where the spot displayed in the gel. [2]Ratio of protein expression levels were calculated with Decyder software as the fold-change between normalized spot volume between VEGF-treated HUVECs and untreated HUVECs. [3]M_w and pI as determined with NCBI database. [4]Number of peptides masses matched/masses riot matched. [5]Protein sequence coverage by peptide mass fingerprinting. [6]The peptides identified with statistically significant ion score.

VEGF stimulation in HUVECs by Western blotting to verify the results of our subcellular proteome analysis. As shown in Figures 1*c* and 1*d*, following the treatment of HUVECs with VEGF, the expression of BiP was significantly elevated in whole cells. This result strongly supported that obtained by 2D-DIGE.

Suppression of VEGF-induced endothelial cell proliferation by BiP knockdown

Although the functional involvement of BiP in angiogenesis has been demonstrated in some reports,[28,29] the role of BiP in VEGF signaling remains unknown. Therefore, we investigated whether BiP is involved in the angiogenic response to VEGF. Endothelial cell proliferation induced by VEGF is an important step in tumor angiogenesis. We examined VEGF-induced proliferation of BiP-knockdown endothelial cells by RNA interference (RNAi). Western blot and real-time PCR analyses revealed that transfection of HUVECs with BiP siRNA (siBiP) successfully suppressed BiP expression in contrast to GFP siRNA (siGFP) transfection (a nonsilencing control) or nontransfection (Figs. 2*a* and 2*b*). The RNAi effect against BiP continued until 96 hr after the transfection (data not shown). A cell proliferation assay with RNAi revealed that the VEGF-induced proliferation of siBiP-transfected HUVECs was significantly suppressed at 24 and 48 hr compared to that of the siGFP-transfected cells (Fig. 2*c*). The ratio of VEGF (+)/VEGF (−), which is considered to indicate the response to VEGF treatment, was significantly suppressed (siGFP, 1.76 ± 0.13; siBiP, 1.12 ± 0.29, $p < 0.05$), suggesting that BiP knockdown may inhibit VEGF-induced cell proliferation.

Inhibition of VEGF-induced MAPK signaling by BiP knockdown

It is reported that VEGF induces endothelial cell proliferation through the activation of the MAPK signal cascade, one of the key cascades in cell proliferation.[30] To clarify whether BiP is associated with the MAPK signaling cascade in response to VEGF, we examined the phosphorylation activity of PLCγ and ERK1/2 in siBiP-transfected HUVECs. VEGF-induced phosphorylation of ERK1/2 and PLCγ was remarkably inhibited in BiP-knockdown HUVECs compared to siGFP-transfected HUVECs without alterations in the total amount of proteins (Figs. 2*d* and 2*e*). Moreover, the phosphorylation of VEGFR-2 (Tyr1175), which is known to be an important region in the activation of PLCγ, was also suppressed in BiP-knockdown HUVECs. Since these results were also obtained with other BiP-targeted siRNA, they did not appear merely to be off-target effects of the siRNA. Thus, BiP may be involved in VEGF signal transduction associated with endothelial cell proliferation through the regulation of phosphorylation of VEGFR-2.

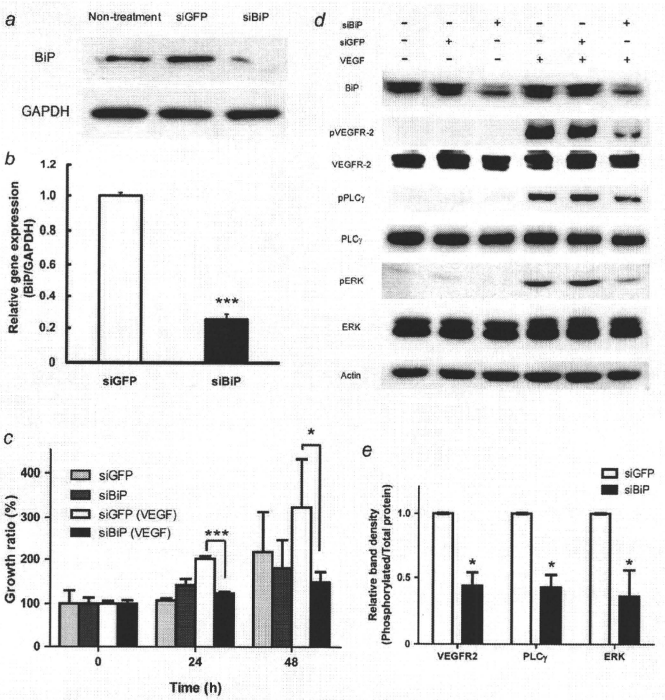

Figure 2. Suppression of VEGF-induced cell proliferation and phosphorylation of VEGFR-2-mediated signal mediators by siRNA knockdown of BiP expression in HUVECs. (*a*, *b*) HUVECs were transfected with BiP siRNA (siBiP) or GFP siRNA (siGFP), and the knockdown effect was analyzed by Western blot and quantitative real-time PCR. (*c*) The cell proliferation assay was performed as follows: The siRNA-transfected HUVECs were seeded (2.0×10^4 cells/well) on a gelatin-coated plate in 0.5% FBS containing EBM-2 medium with or without rhVEGF (20 ng/mL). At the indicated times after incubation, the cell viability was determined with TetraColorOne™. The data indicate the mean ± SD ($n = 3$ or 4), $*p < 0.05$, $***p < 0.001$. (*d*) Phosphorylation of VEGFR-2, PLCγ, and ERK1/2 was analyzed by Western blotting. After serum starvation, the siRNA-transfected HUVECs were stimulated with rhVEGF (20 ng/mL) for 5 or 10 min. Western blotting was performed with antibodies against the indicated proteins. (*e*) The band density was measured with ImageJ software and the densitometric ratio of phosphorylated protein/total protein was calculated. The data was normalized using the ratio for the siGFP (VEGF-treated) group and was indicated as mean ± SEM ($n = 3$), $*p < 0.05$. Similar results were obtained in at least 2 independent experiments.

Increase in cell-surface expression of BiP in HUVECs by treatment with VEGF

It has been shown that in normal tissue cells, BiP is expressed at a low level on the cell surface; however, in certain cancer cells, its expression is upregulated on the surface.[25,31] In the case of angiogenic endothelial cells, it is unclear whether BiP exists on the plasma membrane. Hence, we further analyzed the surface expression of BiP in VEGF-stimulated endothelial cells using a cell-surface protein biotinylation technique.[12,32] As shown in Figure 3*a*, BiP appeared to be abundantly expressed in whole cells of HUVECs, but it was not observed to be present on the surface in contrast to membrane type 1 matrix metalloproteinase, which is known to be expressed on the cell surface (Fig. 3*a*).[17] On the other

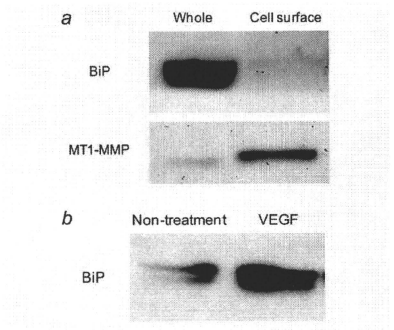

Figure 3. Elevation of BiP expression on the endothelial cell surface by treatment with VEGF. After conjugation of the surface protein with NHS-SS-Biotin, the biotin-conjugated surface proteins were applied to a NeutrAvidin™ column, and eluted with a DTT-containing buffer. (*a*) BiP and MT1-MMP (the latter being a known membrane protein) expressions in whole cell lysate and in the cell surface fraction were detected by Western blot analysis. (*b*) The cell surface expression of BiP in VEGF-treated and nontreated HUVECs was detected by Western blotting. The reproducibility was investigated in an additional independent experiment.

hand, by stimulation of HUVECs with VEGF, BiP expression on the cell surface of the activated cells noticeably increased (Fig. 3*b*).

Characterization of WIFPWIQL liposomes

To investigate the potential of BiP as a target molecule for cancer antineovascular therapy, BiP-targeted peptide-modified liposomes were developed. Previously, it has been reported that DSPE-PEG and peptides can be condensed with the DCC-HOBt method.[33] As indicated in Figure 4*a*, the DSPE-PEG conjugate of GWIFPWIQL-peptides, which are shown to bind to BiP/GRP78,[27] was synthesized. Glycine was used as a spacer amino acid. The synthesized DSPE-PEG-GWIFPWIQL was identified by TLC and ^{1}H-NMR (data not shown). WIFPWIQL liposomes (Fig. 4*b*) were prepared by the freeze-drying method, and the particle size was adjusted by extrusion. TLC analysis confirmed that the lipid derivative of WIFPWIQL peptides was incorporated in the liposomes (data not shown). The size and ζ-potential of the WIFPWIQL liposomes was approximately 120 nm and −50 mV, respectively, and peptide modification did not alter these characteristics as compared to the PEG-modified liposomes (PEG liposomes, as peptide-unmodified liposomes). In addition, we examined the entrapment efficiency of DOX into the liposomes. More than 95% of DOX was detected in both the PEG and WIFPWIQL liposomes.

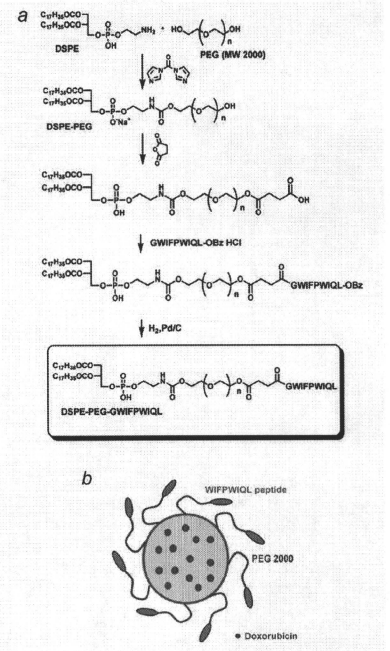

Figure 4. Chemical synthesis of DSPE-PEG-WIFPWIQL. (*a*) The outline of the DSPE-PEG-WIFPWIQL synthesis pathway is illustrated. (*b*) Schematic representation of liposomal doxorubicin modified with DSPE-PEG-WIFPWIQL.

Cellular uptake of BiP-targeted liposomes

To determine whether WIFPWIQL liposomes have a targeting activity, we examined the cellular uptake of the radiolabeled liposomes. WIFPWIQL liposomes were significantly taken up by VEGF-activated HUVECs as well as DU145 in comparison with PEG liposomes (Fig. 5*a*, where WIFPWIQL peptides are shown to bind to the latter cells).[27] Although C26 cells also demonstrated the uptake of WIFPWIQL liposomes, the ratio of the increase was low (1.4-fold) as compared to VEGF-activated HUVECs (5.9-fold).

Intratumoral distribution of WIFPWIQL liposomes

Modification with active targeting tools such as antibodies or peptides has been shown to increase the cellular binding of liposomes and alter their localization in tissues.[34] Since WIFPWIQL-peptide modification is expected to alter their

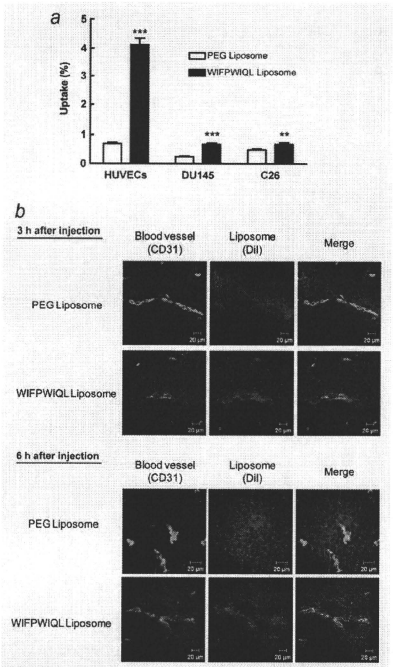

Figure 5. Targeting angiogenic endothelial cells by modification with WIFPWIQL peptides. (*a*) Liposomes were radiolabeled with [^{3}H]cholesteryl hexadecyl ether (370 kBq/mL). The radiolabeled liposomes were added to VEGF-activated HUVECs, DU145, and colon26 NL-17 cells. After incubation for 2 hr at 37°C, the cells were solubilized. The radioactivity of the lysates was measured with a liquid scintillation counter, and the uptake efficiency was calculated. Each bar represents the mean ± SD ($n = 4$). Significant differences in comparison to PEG liposomes are indicated as follows: $^{**}p < 0.01$, $^{***}p < 0.001$. (*b*) Liposomes were fluorescently labeled with DiI C18. Colon26 NL-17-bearing mice were intravenously injected with the labeled PEG liposomes or WIFPWIQL liposomes at day 10 after tumor implantation. At 3 and 6 hr after injection of the liposomes, the tumors were excised; then, frozen tumor sections were prepared. Immunofluorescence staining for CD31 was performed. Green and red portions indicate CD31-positive regions and liposomal distribution, respectively, and yellow portions show the localization of liposomes on vascular endothelial cells. Scale bars represent 20 μm.

localization in tumor tissues, we examined the intratumoral distribution of the peptide-modified liposomes by immunostaining analysis of the endothelial cells in the tumor and fluorescent labeling of liposomes. WIFPWIQL liposomes (red) appeared to be mainly localized in the blood vessels (green) at 3 and 6 hr after injection (Fig. 5*b*). On the other hand, PEG liposomes seemed to leak out broadly from the angiogenic vessels (Fig. 5*b*). In biodistribution study, WIFPWIQL liposomes did not accumulate in normal tissues except spleen where the liposomes accumulated to some extent (data not shown). These findings suggest that WIFPWIQL liposomes actively target tumor vasculature.

Inhibition of tumor-induced angiogenesis by treatment with WIFPWIQL-Lip-DOX

Since WIFPWIQL liposomes could target angiogenic endothelial cells, it is postulated that WIFPWIQL-Lip-DOX selectively inhibits tumor-induced angiogenesis. To assess the antiangiogenic effect of WIFPWIQL-Lip-DOX, we used dorsal air sac model mice.[19] The induction of angiogenesis and the leaking of blood were observed in the dorsal area that was implanted with a chamber ring containing C26 cells (Fig. 6*a*). It appeared that tumor-induced angiogenesis was suppressed by the treatment with WIFPWIQL-Lip-DOX as compared to that with the control and PEG-Lip-DOX (Fig. 6*a*).

Suppression of tumor growth and prolongation of survival time by treatment with WIFPWIQL-Lip-DOX

To investigate the antitumor effect of WIFPWIQL-Lip-DOX, a therapeutic experiment was conducted on C26 cell-bearing mice. WIFPWIQL-Lip-DOX significantly suppressed tumor growth compared to the control and PEG-Lip-DOX (Fig. 6*b*). Since anticancer drugs generally have serious side effects, changes in the body weights of the mice were examined as an indicator of the side effects. After treatment with PEG- or WIFPWIQL-Lip-DOX, although the body weights of the mice were slightly lower than those in the control group, the changes were not significantly different in PEG- and WIFPWIQL-Lip-DOX-treated mice (Fig. 6*c*). Furthermore, WIFPWIQL-Lip-DOX significantly prolonged the survival time of the tumor-bearing mice in comparison with the control and PEG-Lip-DOX-treated groups (Figs. 6*d* and 6*e*).

Expression of BiP in human tumor tissues

To investigate the expression of BiP in actual human tumor tissues, we examined BiP expression in normal and tumor tissues from patients with colon cancer. Angiogenesis plays an important role in colon cancer progression.[35] Bevacizumab (an anti-VEGF monoclonal antibody) and chemotherapeutic medicines are used in colorectal cancer therapy.[36] The expression of BiP was remarkably elevated in the tumor tissues as compared to that in the normal tissues from the same patients (Fig. 7).

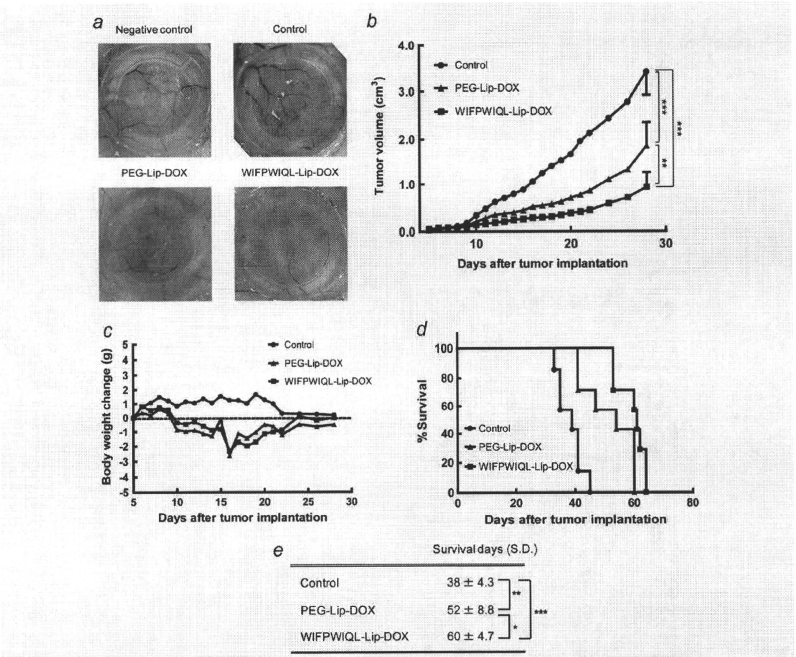

Figure 6. Suppression of tumor growth by treatment with WIFPWIQL-Lip-DOX. (*a*) Antiangiogenic effect of WIFPWIQL-Lip-DOX in dorsal air sac model mice. The chamber rings containing colon26 NL-17 cells (1.0×10^7 cells/150 μL) or medium alone (negative control) were subcutaneously implanted into dorsal skin of BALB/c mice. At days 2 and 3 after implantation with the chamber rings, 0.3 M sucrose solution (control), PEG-Lip-DOX, or WIFPWIQL-Lip-DOX was administered intravenously (5 mg/kg/day). At day 4, the mice were sacrificed, and the dorsal skin that had surrounded the chamber ring was observed. (*b–e*) Colon26 NL-17-bearing mice were intravenously administered with 0.3 M sucrose (control, circle), PEG-Lip-DOX (triangle) or WIFPWIQL-Lip-DOX (square) with a DOX dosage of 5 mg/kg. The tumor volume (*b*), body weight (*c*) and survival time of the mice (*d*, *e*) were monitored. Arrows indicate the day of treatment. Data represent the mean ± SD ($n = 7$). Significant differences in tumor growth and survival were analyzed by ANOVA with Tukey's *post-hoc* test and log-rank test, respectively, and are indicated as follows: $^*p < 0.05$, $^{**}p < 0.01$, $^{***}p < 0.001$. A similar result was obtained in another independent experiment.

Discussion

We herein describe the application of 2D-DIGE technology to subcellular proteome analysis to analyze the protein expression profile between VEGF-stimulated endothelial cells—as an angiogenesis model—and nonstimulated endothelial cells. Although VEGF-stimulated endothelial cells may not completely reflect angiogenic endothelial cells in tumors, VEGF is the most important proangiogenic factor. Moreover, VEGF-stimulated endothelial cells are commonly used as a representative model in investigations of angiogenesis. In previous studies, VEGF-regulated cellular molecules have been partially characterized by DNA microarray[37] or proteomic analysis using conventional 2D electrophoresis.[38] Subcellular proteomics is probably a more powerful tool for the identification of organelle proteins and is expected to further the discovery of functional molecules.[10,12,39] Using subcellular proteomics, we found that the expression of many proteins was considerably altered in angiogenic endothelial cells